THE STATE-SWITCHED ABSORBER USED FOR VIBRATION CONTROL OF CONTINUOUS SYSTEMS

A Dissertation
Presented to
The Academic Faculty

By

Mark Horner Holdhusen

In Partial Fulfillment
Of the Requirements for the Degree
Doctor of Philosophy in Mechanical Engineering

Georgia Institute of Technology
February 2005

THE STATE-SWITCHED ABSORBER USED FOR VIBRATION CONTROL OF CONTINUOUS SYSTEMS

Approved by:

Dr. Kenneth Cunefare, Advisor
School Mechanical Engineering
Georgia Institute of Technology

Dr. Sathyanaraya Hanagud
School of Aerospace Engineering
Georgia Institute of Technology

Dr. Nader Sadegh
School of Mechanical Engineering
Georgia Institute of Technology

Dr. Massimo Ruzzene
School of Aerospace Engineering
Georgia Institute of Technology

Dr. Also Ferri
School of Mechanical Engineering
Georgia Institute of Technology

Date Approved: February 2005

ACKNOWLEDGMENTS

Obviously, completing a huge task like researching and writing a dissertation is nothing I could do by myself. Many people have helped me over the last five-plus years to get through this process known as a Ph.D. Some have helped with professional advisement and encouragement, while others given me unconditional love and support during these years and the rest of my life.

First of all, I need to thank my advisor, Dr. Cunefare, for his guidance and support through these last few years. Your knowledge and experience set me on the right path and kept me there. You were more than just an academic advisor; you are a role model for how conduct yourself in an academic and professional setting. The amount I have learned from Dr. C. is immeasurable.

I also need to thank my Ph.D. reading committee, Dr. Sadegh, Dr. Ferri, Dr. Ruzzene, and Dr. Hanagud. I appreciate the time and input you've given to this process. Also, I need to thank all of my fellow students that work for Dr. Cunefare. You all have helped me get through those tough times we've all experienced with a smile on my face and some amount of dignity. Specifically, I need to thank (Dr.) Wayne Johnson. Your leadership and experience made my time at Georgia Tech just a little simpler. Watching you go through this process ahead of me helped me learn to do and what not to do.

The emotional support system I have made the last several years tolerable. All my friends and family were there whenever I needed them and for this I am forever grateful. The support I received over the years from my wife, Elona's, family was truly amazing. You accepted me as your son and brother and treated as if I had grown up with you since birth. Your unconditional love and support is one of the truly special relationships in my life and I will always cherish what you have given me.

I could not have done this without the support of my brother and his family. David, you are the single most important role model in my life. I stand in awe everyday of who you are and what you accomplish and I count my blessings each and every morning that you are my big brother. For the first time, I have completed a task before you and I am honored that I can finally repay you with any advice and support you may need while completing your Ph.D.

What would a man be without his parents? Mom and Dad, I owe my desire to learn solely to you. The support, guidance, and discipline you gave me growing up set me on the right path in life, both mentally and emotionally. You instilled the importance of education in me that has kept me going for the last 22 years. Mom, without your years of making my papers bleed red ink, I could have never completed a document of this length. Dad, my curious nature comes from all those times watching you take my broken toys apart and making them better and more durable than when they came out of the box. I owe the both of you for making me the man I've become.

Finally, there is no way I could possibly thank my wife Elona enough. Elona, you are the most patient, caring, loving, strong, independent, funny woman that I know. You are the reason I do what I do and am what I am. You are my rock during the hard times (i.e. qualifiers) and my cheerleader during the high times (i.e. right now). The most amazing thing is you do this all while making your own list of impressive accomplishments. You truly amaze and inspire me. This is a true partnership and one that I consider myself lucky of which to be a part. We did it! And I truly mean we, as without you I would probably be sitting in a cubicle somewhere hating my life. This is just the beginning and I can't wait to see where this journey takes us. I love you more than any acknowledgment page could ever say.

TABLE OF CONTENTS

ACKNOWLEDGMENTS iii

LIST OF TABLES vii

LIST OF FIGURES viii

SUMMARY xi

CHAPTER 1: INTRODUCTION 1

Previous Absorber Research 1

State-Switched Absorber Development 5

Research Objectives 9

CHAPTER 2: STATE-SWITCHING CONCEPTS 11

Dynamics 11

Switching Criteria 12

CHAPTER 3: SWITCHING RULE INVESTIGATION 15

Maximum Work Extraction 15

Stability 22

Switch Timing 26

Delayed Switched 26

Ramped Switch 30

CHAPTER 4: EQUATIONS OF MOTION 33

Cantiliever Beam 33

Clamped Plate 37

CHAPTER 5: STATE-SWITCHED ABSORBER OPTIMIZATION 41

Optimization Method 41

Beam Optimization Results 44
Plate Optimization Results 53
CHAPTER 6: EXPERIMENTAL SETUP 61
State-Switched Absorber Design 61
Beam and Plate Setup 64
Beam Setup 64
Plate Setup 66
Instrumentation 68
Procedures 71
Beam Procedures 71
Plate Procedures 75
CHAPTER 7: EXPERIMENTAL VALIDATION RESULTS 77
Beam Results 77
Plate Results 82
CHAPTER 8: CONCLUSIONS 86
REFERENCES 90

LIST OF TABLES

TABLE

6.1: SSA tuning frequencies and forcing frequencies for both beam experiments..... 72

6.2: SSA tuning frequencies and forcing frequencies for the plate experiments..... 75

LIST OF FIGURES

FIGURE

2.1: Model of state-switched dynamical device 11

3.1: Ratio, in dB, of base kinetic energies of an SSA to a TVA for a two-frequency excitation. Negative dB values indicate better performance of the SSA. 16

3.2: Ratio, in dB, of input power of an SSA to a TVA for two-frequency excitation 18

3.3: Ratio, in dB, of dissipated power of the SSA damper to the base damper 20

3.4: Ratio, in dB, of dissipated power of the TVA damper to the base damper 21

3.5: Phase portrait of a single stiffness state 23

3.6: Switching rule for unstable example 24

3.7: Trajectory of an unstable switched system 24

3.8: Phase portrait of maximum work extraction switching rule 25

3.9: Phase portrait of a state switching system with a delayed instantaneous switch 28

3.10: Phase portrait of state switching system with ramped stiffness switch 31

4.1: State-Switched absorber attached to a beam, subject to multi-harmonic point forcing 33

4.2: State-switched absorber attached to a plate, subject to multi-harmonic point forcing 37

5.1: Kinetic energy ratio, in dB, of an optimized SSA system to an untreated beam as function of two forcing frequencies 45

5.2: Kinetic energy ratio, in dB, of an optimized SSA to an optimized TVA as function of two forcing frequencies 46

5.3: Optimum SSA location along a beam as function of two forcing frequencies 47

5.4: Mean of two SSA tuning frequencies normalized by first mode of beam as function of two forcing frequencies 48

5.5: Ratio of optimum SSA tuning frequencies as function of two forcing frequencies .. 49

5.6: Kinetic energy ratio of SSA to optimized TVA as a function of tuning parameters near the best performing SSA 51

5.7: Kinetic energy ratio of SSA to optimized TVA as a function of tuning parameters near average performing SSA 53

5.8: Kinetic energy ratio, in dB, of an optimized SSA system to an untreated plate as function of two forcing frequencies 54

5.9: Kinetic energy ratio, in dB, of an optimized SSA plate system to an optimized TVA plate system as function of two forcing frequencies 55

5.10: Optimum SSA location in the x direction on the plate as function of two forcing frequencies 57

5.11: Optimum SSA location in the y direction on the plate as function of two forcing frequencies 57

5.12: Mean of two SSA tuning frequencies normalized by first mode of plate as function of two forcing frequencies 58

5.13: Ratio of optimum SSA tuning frequencies for a plate as function of two forcing frequencies 59

6.1: MR elastomer implementation of a state-switched absorber. 62

6.2: SSA resonance frequencies as a function of electromagnet current 63

6.3: Frequency response of cantilever aluminum beam 65

6.4: Frequency response of cantilever steel beam 66

6.5: SSA frequencies versus current for plate experiments 67

6.6: Frequency response of plate 68

6.7: Experimental setup with sensors and actuators 69

6.8: Plate layout including accelerometers, force transducer, and SSA locations. 70

7.1: Experimental kinetic energy ratio, in dB, of the aluminum beam with SSA attached to untreated beam. Forcing frequencies near first mode of vibration. 78

7.2: Experimental kinetic energy ratio, in dB, of the steel beam with SSA attached to untreated beam. Forcing frequencies near second mode of vibration..... 79

7.3: Experimental kinetic energy ratio, in dB, of beam with SSA attached to beam with TVA attached. Forcing frequencies near first mode of vibration. 80

7.4: Experimental kinetic energy ratio, in dB, of beam with SSA attached to beam with TVA attached. Forcing frequencies near second mode of vibration..... 81

7.5: Experimental kinetic energy ratio, in dB, of the plate with SSA attached to untreated plate. 83

7.6: Experimental kinetic energy ratio, in dB, of a plate with SSA attached to a plate with TVA attached. 84

SUMMARY

A State-Switched Absorber (SSA) is a device capable of instantaneously changing its stiffness, thus it can switch between resonance frequencies, increasing its effective bandwidth as compared to classical tuned vibration absorbers for vibration control. This dissertation considers the performance of the SSA for vibration suppression of continuous systems, specifically a beam and a plate. The SSA tuning frequencies and attachment point on the continuous body were optimized using a simulated annealing algorithm. It was found that an optimized SSA outperforms and optimized TVA at controlling vibrations of both a beam and a plate. These performance gains were also observed experimentally employing magneto-rheological elastomers to achieve a stiffness change. This dissertation also considers zero strain switching criteria and the maximum work extraction switching rule used by the SSA. The zero strain switching criteria ensures the system remains stable as no energy is added or released across a switch event. The maximum work extraction switching rule is designed to maximize the power dissipated by the absorber, but also guarantees minimization of the motion of the base to which the absorber is attached.

CHAPTER 1

INTRODUCTION

This research considers the theoretical optimization and experimental validation of a state-switched absorber (SSA) used in continuous systems. An SSA is a variation of the classical tuned vibration absorber that is capable of instantaneously changing from one discrete stiffness to another. Altering the stiffness element of the absorber instantaneously changes the resonance frequency of the device. State switching can provide performance gains over classical vibration absorbers, especially for excitations with more than one frequency component.

The first section in this chapter contains a discussion of previous research in the area of vibration absorbers. That will be followed by a review of the research that led directly to the development of the state-switched absorber. The chapter concludes with a brief overview of prior work investigating the state-switched absorber used for vibration control.

PREVIOUS ABSORBER RESEARCH

The state-switched absorber (SSA) is related to many types of vibration absorbers, including classical passive absorbers as well as adaptive and active absorbers. Sun et al. [1] give an extensive overview of the origin, design, and applications of numerous vibration absorbers. Many of the absorber concepts discussed in the following literature review are detailed in the paper by Sun et al. Sun et al.'s paper is an excellent review of tuned vibration absorbers and variants through 1995 and interested readers may find more

extensive references in the Sun article than those key, selected papers and developments discussed below.

There are two classical passive vibration control devices, the tuned vibration absorber (TVA) and the tuned vibration damper (TVD). While these two devices are similar, they serve different functions. The TVA theoretically brings the base to which it is attached to rest at a single excitation frequency, the resonance frequency of the TVA.[2] The TVA is classically used to suppress a single harmonic excitation on vibrating systems. The TVA is a lightly damped mass-spring device with a mass much smaller than the mass to which it is attached. The natural frequency of the TVA is tuned to that of the excitation frequency. It can be shown, that designing the TVA in such a way results in no motion in the base mass to which the TVA is attached. While the TVA works for a single excitation frequency, resonances in the system appear just above and below the excitation frequency, making the TVA's effective bandwidth very narrow. By introducing damping to the absorber, these resonant peaks can be reduced, thus increasing the effective bandwidth of the device. However, the introduction of damping decreases the effectiveness of suppressing base vibration at the absorber's resonance frequency.

While TVAs are designed to reduce the base motion near a specific frequency, a TVD is designed to increase the energy losses due to the damping in the system.[3] To achieve maximum damping losses in the structure, the TVD maximizes the relative velocity across its damping element. Maximizing the energy losses does not guarantee the minimization of base motion at the attachment point. Unlike the TVA, the TVD is

not designed to control the response of only one frequency of vibration, thus it may be made effective over a range of frequencies.

Classical passive absorbers are tuned for set operating conditions. These operating conditions can change over time and cause the absorber to become ineffective and potentially increase the base vibration. Adaptive tuned vibration absorbers (ATVAs) overcome this through an algorithm that tunes the absorber as conditions change.[1] Since the ATVA is capable of changing its resonance frequency, it has an increased effective bandwidth over classical devices. Adaptive tuning approaches tune to only a single frequency for each operation.[4, 5] Using closed-loop control, adaptive tuned vibration absorbers can also be used for purposes other than just local vibration suppression, such as noise control.[4] To achieve a change in resonance frequency, the properties of an ATVA may be modified using either active or semi-active control of the device.

Active control allows for the direct control of the absorber's transmitted force as well as modifying the dynamic properties of the device. This is achieved using force actuators that require external energy and system feedback. Initial research in active adaptive tuned vibration absorbers considered a force actuator in parallel with the absorber's stiffness and damping elements.[6-8] Using closed-loop control, the force actuator essentially modified the effective stiffness and damping of the absorber. Dosch et al.[8] used these active control concepts to develop an inertial piezoceramic force actuator. More recently, adaptive filtering methods were used to control the force actuator which improved the performance of the absorber.[9, 10] The advantage of using active control is it allows for fast response to disturbances. Some disadvantages to active

control techniques are the potential for large actuator forces which may require high power inputs, increased complexity in the system, and the possibility of instability.[5]

A semi-active absorber achieves vibration control by changing its dynamic parameters, such as the stiffness or damping. Some advantages of semi-active control are it requires less energy, costs less, and has reduced complexity versus active systems, while being nearly as effective. The state-switched absorber is more closely related to semi-active control concepts described below since only the system's dynamic parameters are modified with no active forcing actuator. Walsh and Lamancusa[11] reduced transient vibrations using a mechanically variable spring. Lai and Wang[12] integrated a closed-loop controller to enhance the performance of the variable stiffness concept of Walsh and Lamancusa. Further advancing the variable parameter concept, the addition of a variable damping element into a feedback controller improved the performance of the absorber under transient vibration conditions.[13, 14] Nguyen[15] explored parametric excitation as a tool for vibration control. Parametric excitation generates a secondary harmonic excitation by varying the coefficients of the equations of motion. While parametric excitation reduces resonances, it is not effective for broadband vibration control.[15] A variable damping element that produces a force proportional to the absolute absorber velocity is termed a sky-hook damper.[16] Bender[16], Krasnicki[17], and Karnopp[18] all used this concept of the sky-hook damper to reduce vibrations through semi-active control. The sky-hook damper requires only a small amount of energy to adjust the damping force. As compared to passive dampers, the semi-active sky-hook damper can further reduce the vibration transmission across the suspension to which the vibrating body is attached. The sky-hook concept has mainly

been researched for semi-active vehicle suspensions.[19-23] Gavin and Doke [24] used a control rule similar to the sky-hook concept to control seismic vibration in a base-isolated building using both variable damping and variable stiffness devices.

Optimization of a vibration absorber is needed to minimize the vibration in the system to which it is attached. Den Hartog [2] optimized the classical damped vibration absorber by altering the damping to minimize the amplitude peaks in the frequency response function. Research has also been conducted optimizing the tuning parameters of vibration absorbers applied to continuous systems. Jacquot[25] modeled a continuous beam as a one-degree of freedom and the optimum absorber parameters were determined for this equivalent lumped mass system. To minimize the response for the first two modes, Kitis et al.[26] employed a gradient-based optimization to tune two TVAs attached to a cantilever beam. Rice[27] used a SIMPLEX algorithm to optimize the position, stiffness, and damping of absorbers attached to a beam. Esmailzadeh and Jalili[28] fixed the absorbers' position along the beam and optimized their stiffness and damping by means of a Direct Update Method. A genetic algorithm was used by Hadi and Arfiadi[29] to optimize the parameters of a tuned vibration absorbers applied to multi-degree-of-freedom structures.

STATE-SWITCHED ABSORBER DEVELOPMENT

Davis et al.[30] recognized that the piezoceramic device developed by Dosch et al.[8] could be considered as a controllable variable stiffness element, due to the dependence of the piezoceramic's stiffness on the output impedance. Clark[31] and Richard et al.[32] have considered piezoelectric devices for state-switched vibration control. The switching criteria used by both Clark[31] and Richard et al.[32] allow for

switching at maximum displacement across the stiffness element to optimize the dissipation of energy. However, switching at maximum strain will cause undesirable mechanical transients in the system.[33-36] Mechanical transients, as stated here, are shocks in the response due to a sudden release or addition of energy to the system violating the conservation of energy principle. State-switched systems are not, in general, stable.[37] Certain switching laws can lead to an energy addition to the system, which can cause the system to become unstable.[37]

The state-switched absorber was directly derived from a device designed by Larson et al.[33-35] for use in underwater transduction. The state-switched transducer has the same fundamental concept as the SSA in that it is capable of instantaneously switching between discrete stiffnesses. Switching between discrete stiffnesses changes the resonance frequency of the device, thus increasing the effective bandwidth.

The state-switched transducer uses piezoelectric material as the spring element in the system. The piezoelectric configuration used by Larson et al.[33-35] is similar to the approach used by Davis and Lesieutre,[5, 38] except Davis and Lesieutre's device was implemented for vibration control, whereas Larson's objective was underwater transduction. The stiffness of a piezoelectric element is different when it is short circuited as compared to when it is open circuited.[30, 38] If the piezoelectric circuit can be controlled, switching the stiffness of the piezoelectric material can occur as fast as the circuit can be changed. If the instantaneous change in stiffness occurs at zero strain, then no mechanical transients will be introduced to the system. Switch events can potentially occur every half-cycle of oscillation of the state-switched device.

Piezoelectric elements have a relatively high stiffness, which can lead to relatively large absorber masses. Also, piezoelectric materials should not be put into tension, as they are fragile and have displacement amplitude limitations. To make the device more robust and lower the absorber mass, magneto-rheological (MR) elastomers could be implemented as a variable spring element.[39] An MR elastomer is a polymer with fine iron particles suspended in it. The stiffness of an MR elastomer depends on the magnetic flux across it.[39] Since the MR elastomer is composed of rubber as opposed to ceramic, the stiffness will be much lower than a piezoelectric material, thus resulting in a smaller mass for a similar resonance frequency.

Cunefare et al.[40] conducted introductory research on the state-switched absorber used for vibration control. Their work focused on state-switching theory and theoretical simulations of simple one-degree of freedom and two-degree of freedom systems. For the single degree of freedom system, an SSA with two discrete stiffnesses was compared to two passive tuned vibration absorbers (TVA) excited by an identical base motion. Cunefare et al.[40] found that the SSA dissipates more work than the TVAs, illustrating a greater damping capability in the SSA. Also, as the spacing in excitation frequencies increased, the relative performance of the SSA increased as compared to the TVAs. Therefore, the SSA has a larger effective bandwidth as compared to the classical TVA.

The second system investigated by Cunefare et al.[40] was a simple two-degree of freedom system. A single two-state SSA was compared to a single TVA attached to identical bases with identical two-frequency component forcings. The SSA did as well as or outperformed the TVA for all combinations of excitation frequencies investigated,

including single frequency excitations. As in the single-degree of freedom system, the comparative performance of the SSA increases as the spacing between forcing frequencies increases, illustrating a broader effective bandwidth. The significance of the simulations is that the SSA has the potential for performance gains as compared the classical passive TVAs.

Holdhusen[41] also researched the SSA considering the role of damping and its effect on the vibration control performance and modeling of the state-switched absorber. The SSA was found to be most effective at low damping values. Also, changing the models of damping does not have a significant effect on the final performance of the SSA as compared to a TVA.

Holdhusen[41] also examined the experimental validation of the state-switched absorber. The state-switched absorber was implemented using magneto-rheological fluid and a collection of coil springs. The SSA showed performance gains experimentally as compared to classical tuned vibration absorbers. Also, the SSA was observed to be effective over a larger bandwidth than that of a classical TVA. The damping in the SSA system examined by Holdhusen[41] was time variant due to the temperature change of the MR fluid used to implement switching. Therefore, the damping could not be exactly determined during the operation of the SSA system and the response could not be modeled.

The state-switched absorber is very similar to classical tuned vibration absorbers. The fundamental difference between the SSA and the TVA is that the TVA is tuned to only one frequency at which the system operates, whereas the SSA is capable of switching between discrete resonance frequencies while the system operates. At any

instant in time during operation, the SSA acts at only one discrete frequency, but when a switch event occurs the resonance of the absorber instantaneously changes and acts at a different frequency until the next switch event. The switching of resonances increases the effective bandwidth of the absorber.

The ability of the state-switched absorber to change stiffness classifies it as a form of semi-active vibration control. While the SSA is related to adaptive tuned vibration absorbers, the adaptive tuned vibration absorber is only effective at an adaptively tuned single frequency as opposed to the SSA effectiveness at multiple frequencies. The state-switched absorber's ability to switch between resonance frequencies and broaden its effective bandwidth is what differentiates it from prior vibration absorber technologies.

RESEARCH OBJECTIVES

The research detailed here will investigate the performance of the state-switched absorber used for controlling the vibration of continuous systems. The switching rule employed to reduce vibrations will be investigated for its robustness and limitations. Also, the tuning and attachment location for the SSA will be optimized for both beam and plate systems. The performance of the optimized SSA will be compared to that of an optimized classical TVA. The results from this theoretical optimization will be validated experimentally.

This dissertation will continue by outlining the basic dynamics and switching criteria employed in the state-switched absorber. The investigation of the switching rule implemented is then detailed. Next, the governing equations of motion for the systems considered are outlined, followed by a discussion of the optimization of the SSA applied to continuous systems. Then, the experimental setup and results of the SSA applied to a

beam and plate are described. This dissertation will end by drawing some conclusions from this research.

CHAPTER 2

STATE-SWITCHING CONCEPTS

In the following sections, the basic tools required to analyze and simulate a state-switched absorber attached to various dynamic systems are developed. These tools are meant to be general and not specific to a particular hardware implementation of state switching. The only restrictions on the analysis is that the absorber's spring stiffness is the sole switchable property, and switching only occurs at zero relative strain across the switchable spring.

DYNAMICS

Figure 2.1 depicts a model of an SSA. The SSA in isolation is a single degree of freedom spring-mass-damper device. The arrow through the spring in Figure 2.1 implies a spring with selectable, discrete stiffnesses. The SSA has as many states as it does discrete stiffnesses. For the work at hand, the SSA will have only two potential stiffness states, k_1 and k_2, where $k_1<k_2$.

Each discrete stiffness yields a distinct, discrete resonance frequency,

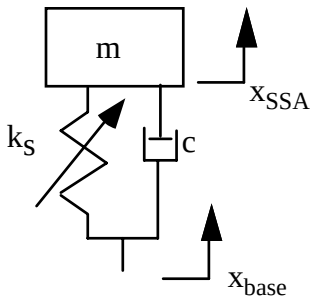

Figure 2.1: Model of state-switched dynamical device

$$\omega_i = \sqrt{k_i / m}\,. \tag{2.1}$$

Notice that the SSA in isolation has only one observable resonance frequency at any given time. The observable state of the SSA is called the 'on-line' state. Thus, the 'off-line' state is the other potential state of the SSA. When a switch in state occurs the 'on-line' stiffness becomes the 'off-line' stiffness and vice versa. For example, if the 'on-line' state has the stiffness k_1 and its corresponding resonance ω_1, a switch event at zero relative displacement will cause the stiffness to change to k_2, thus changing the resonance to ω_2.

SWITCHING CRITERIA

To avoid mechanical shocks in the system response, switching should only occur at zero relative displacement across the SSA, which is determined by

$$z = x_{SSA} - x_{base} = 0\,, \tag{2.2}$$

where x_{SSA} is the displacement of the absorber and x_{base} is the displacement of the base. When the relative displacement across the spring is zero there is no potential energy in the spring (it is presumed that there is no static pre-load in the spring), thus the energy before and after the switch event remains equal. Since the energy before the switch is equal to the energy after the switch, there is no energy input needed to the system and thus the system will remain stable.[37] If a switch event occurs when the relative displacement is non-zero, the spring contains some potential energy that is instantaneously released, causing shocks in the response of the system.

Zero strain across the spring is a necessary condition for switching to occur, however, the system need not switch at every occurrence of zero relative displacement. The fundamental question is whether or not to switch at a switch opportunity. For the work previously done by Cunefare et al. [40] and Holdhusen[41], a maximum work extraction principle was implemented. To achieve a maximum work extraction in a two state SSA, the switching rule is

$$k_{SSA}^{\ next} = \begin{cases} k_{SSA1} \ \text{if} \ \ \dot{x}_{base}(\dot{x}_{SSA} - \dot{x}_{base}) > 0 \\ k_{SSA2} \ \text{if} \ \ \dot{x}_{base}(\dot{x}_{SSA} - \dot{x}_{base}) < 0 \\ k_{SSA} \ \text{if} \ \ \dot{x}_{base}(\dot{x}_{SSA} - \dot{x}_{base}) = 0 \end{cases}, \tag{2.3}$$

where $k_{SSA}^{\ next}$ is the next value of the stiffness. The switching rule described by (2.3) results in a maximum work extraction by the absorber, but does not guarantee minimized base motion. The SSA behaves somewhat like a vibration damper under the switching rule described. A physical interpretation of the switching rule is that when the force exerted by the SSA on the base opposes the base motion, a stiffer spring removes more energy from the base. Likewise, a softer spring puts less energy into the base during periods when the SSA force acts in the same direction as the base motion. It is noted that the switching logic defined by Equation (2.3) is closely related to the 'sky hook' optimal damping concept.[16-18]

Since the SSA can only be in one state at any given time, the modeling of the SSA is quite simple. Between switch events, the SSA exhibits only one stiffness, thus behaves like a classical vibration absorber at any given time. When implemented into a simulation, the equations of motion must be changed at each switch instant in order to reflect the dynamic properties of the 'on-line' state of the system. After each switch event, the absorber is tuned to a new resonance frequency and acts like a classical TVA

with an initial velocity and displacement equaled to the final velocity and displacement before switch event. After each switch event, the solution to the differential equation of motion is the sum of the particular solution and the homogeneous solution of the differential equation. The particular solution is calculated from the excitation of the system, whereas the homogenous solution is the free response of the system and thus depends on the initial conditions. There is a start-up transient after each switch event due to the dependence of the homogeneous solution on the initial conditions that are present after the switch. Because this transient occurs at every switch event, the system can never reach a steady-state condition due to recurrent switching during the response. Since the system never reaches steady state, a frequency response function cannot be calculated for the SSA response. Also, due to the non-linearity of the switching, superposition does not hold and the addition of the frequency response functions of a TVA at two frequencies will not result in that of the SSA.

CHAPTER 3

SWITCHING RULE INVESTIGATION

This chapter discusses the state-switched absorber switching criteria and rule detailed in the previous chapter. The switching rule is investigated to gain a better understanding of how the SSA works and how robust the switching rule is. The chapter begins with a discussion of the maximum work extraction switching rule and the physics behind why the SSA outperforms passive devices. Then, the stability of the vibrating system subjected to the zero relative displacement switching criteria is considered. Finally, the effect inaccurate switch timing has on SSA performance is considered, including delayed switching and ramped switching.

MAXIMUM WORK EXTRACTION

The state-switched absorber used for vibration control uses the maximum work extraction switching rule defined by Equation (2.3). This switching rule was developed by Cunefare et al. [40] and is designed to maximize the work extracted from the base to which the absorber is attached. Maximizing the extracted work does not, however, guarantee reduced vibrations in the system trying to be controlled. As Cunfare et al. [40] showed, as will be showed later in this dissertation, reduced base motion is a byproduct of this switching rule.

To determine what occurs for the maximum work extraction switching rule to result in reduced vibrations in the base, the research performed by Cunefare et al. [40] must be reviewed. In this paper, the switching criteria and rule were derived and simulations were performed for the SSA applied to an elastically mounted lump mass.

The performance of the SSA was compared to that of a TVA for a base mass subjected to an excitation with two frequency components of equal amplitude. Both absorbers tuning frequencies were optimized using a direct search algorithm for a range of excitation frequency combinations. The metric of performance for this system was defined to be the kinetic energy of the base mass. The lower the base kinetic energy, the better the performance of the absorber. Figure 3.1 shows the ratio of base kinetic energy of the optimized SSA to the base kinetic energy of the optimized TVA as a function of the two excitation frequencies. The energy ratio is represented in dBs, therefore when the value is negative the SSA performs better than the TVA. The forcing frequencies have been normalized by the natural frequency of the isolated base system. Figure 3.1 has a larger range of forcing frequencies than was presented in the original paper. As can be seen, the

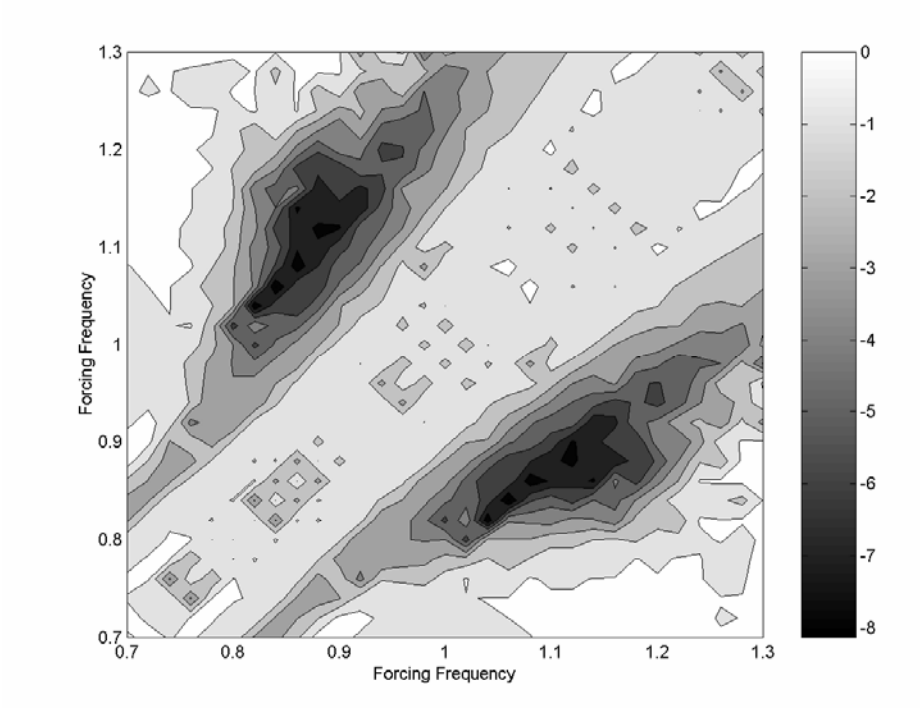

Figure 3.1: Ratio, in dB, of base kinetic energies of an SSA to a TVA for a two-frequency excitation. Negative dB values indicate better performance of the SSA.

ratio value is negative for the entire range of forcing frequencies considered, therefore the SSA outperforms the TVA for all excitation combinations considered. Note, there is a smaller range of forcing frequencies where the SSA performs at its best as compared to a TVA.

To determine what happens in the SSA that results in improved performance over a TVA, a power balance of the system is considered. The power balance law for a vibratory system is

$$\dot{T} + \dot{V} = P_{in} - P_{out} \tag{3.1}$$

where T is kinetic energy, V is potential energy, P_{in} is power input by external forces, and P_{out} is work dissipated by the dampers in the system. To dissect this power balance, the power is averaged over one period of repetition in the response of the system. The time rate of change of kinetic energy and potential energy averaged over one repetition period is zero. Therefore, the dampers must dissipate all the input power to the system for the power balance in Equation (3.1) to remain true. The work dissipated by the system dampers is

$$P_{out} = c_{base}\dot{x}_{base}^2 + c_{abs}\left(\dot{x}_{abs} - \dot{x}_{base}\right)^2 \tag{3.2}$$

where c_{base} and c_{abs} are the damping coefficients of the base and absorber, respectively, and x_{base} and x_{abs} are the displacements of the base and absorber, respectively. The input power is

$$P_{in} = \left[F_1 \sin\left(\omega_1 t\right) + F_2 \sin\left(\omega_2 t\right)\right]\dot{x}_{base} \tag{3.3}$$

where F_1 and F_2 are the forcing amplitudes, ω_1 and ω_2 are the forcing frequencies, and t is time. Note, this input power is a function of the velocity of the base, which has both

amplitude and phase. The phase of the base response is dependent on both resonance frequencies and damping in the system. Therefore, switching between resonance frequencies in the SSA can change the response phase and may result in an increased or decreased power input, without necessarily changing the vibration amplitude.

To determine the effect switching has on the power input, a state switching system is compared to a system without switching, i.e. a tuned vibration absorber system. Figure 3.2 the ratio of input of the SSA to the TVA for a range of two-frequency component forcings. The absorber tunings used to create Figure 3.2 are identical to the optimized tunings found to create Figure 3.1. For each forcing combination, the input power was determined for each absorber and time averaged over one period of repetition in the system response. The ratios of the SSA input power to the TVA input power are

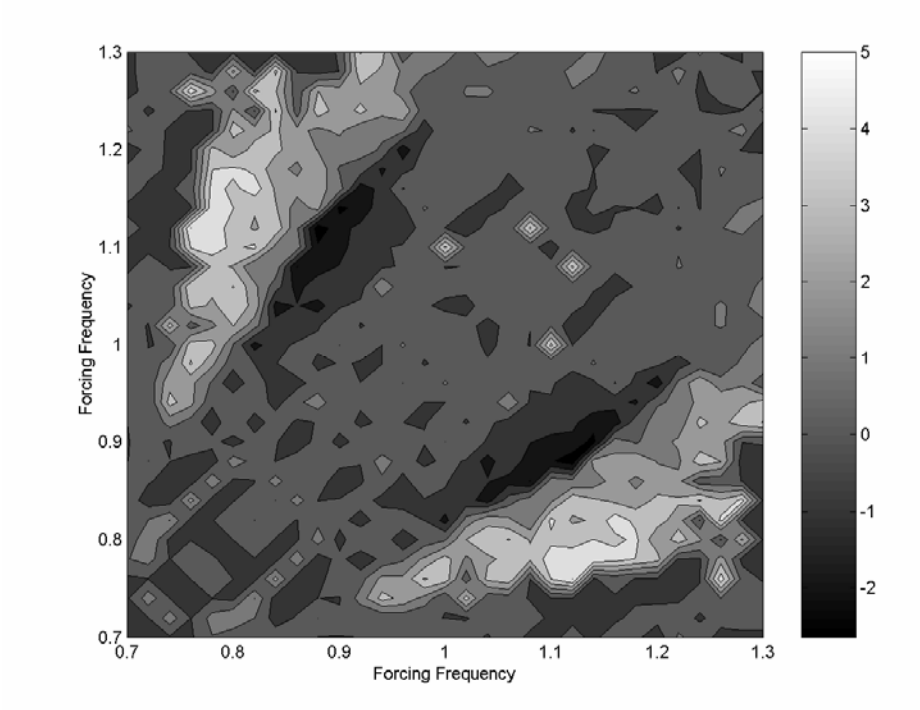

Figure 3.2: Ratio, in dB, of input power of an SSA to a TVA for two-frequency excitation

displayed, in decibels, in Figure 3.2. For the majority of the forcing cases considered, the ratio value is zero indicating that switching has little effect on the power input for most of the cases considered. The lowest power input ratio occurs for the same forcing case that results in the best relative performance of the SSA, depicted in Figure 3.1. For this case, there is 2.5 dB less input power in the SSA system than in the TVA system and the SSA dampers do not need to dissipate as much work as the TVA dampers. The highest input power ratio occurs at a point of low relative performance of the SSA. In this case, there is a 5 dB increase of power input to the SSA system as compared to the TVA system resulting in more work dissipation in the SSA's dampers. As Figure 3.1 shows, the SSA outperforms the TVA for this forcing case, demonstrating that the SSA was able to reduce base motion in spite of the increased power input to the system.

To determine how the SSA works to reduce the motion, even for increased power inputs, the power dissipation in each damper must be examined. Focusing on the power dissipated in the base system's damper and that dissipated in the SSA's damper in Equation (3.2), the following equations are obtained,

$$\begin{aligned} P_{out,base} &= c_{base}\dot{x}_{base}^2 \\ P_{out,abs} &= c_{abs}\left(\dot{x}_{abs} - \dot{x}_{base}\right)^2 \end{aligned} \tag{3.4}$$

where $P_{out,base}$ is the power dissipated by the damper between the base and ground and $P_{out,abs}$ is the power dissipated by the damper. Minimizing the power dissipation in the base damper results in minimizing the base vibration, as this dissipation depends only on the base velocity and a damping coefficient. Conversely, maximizing the power dissipated by the absorber's damper will also result in minimizing the base motion since all the power input to the system must be dissipated by both system dampers.

Maximization of the power dissipated by the absorber's damper is exactly what the maximum work extraction switching rule does.

To show that the SSA damper dissipates most of the power added to the system, reducing the motion of the base, the work extracted by each system damper must be compared. Figure 3.3 depicts the ratio, in dBs, of the work extracted by the state-switched absorber's damper to that of the base damper for the same forcing and tuning cases used for Figures 3.1 and 3.2. When this value is greater than zero, the absorber damper dissipates more power than the base damper. For nearly the entire range excitation frequencies, the ratio value is greater than zero dB and therefore the absorber damper dissipates more power than the base damper. Only a very small range of forcing frequencies had a higher power dissipation in the base damper than in the absorber

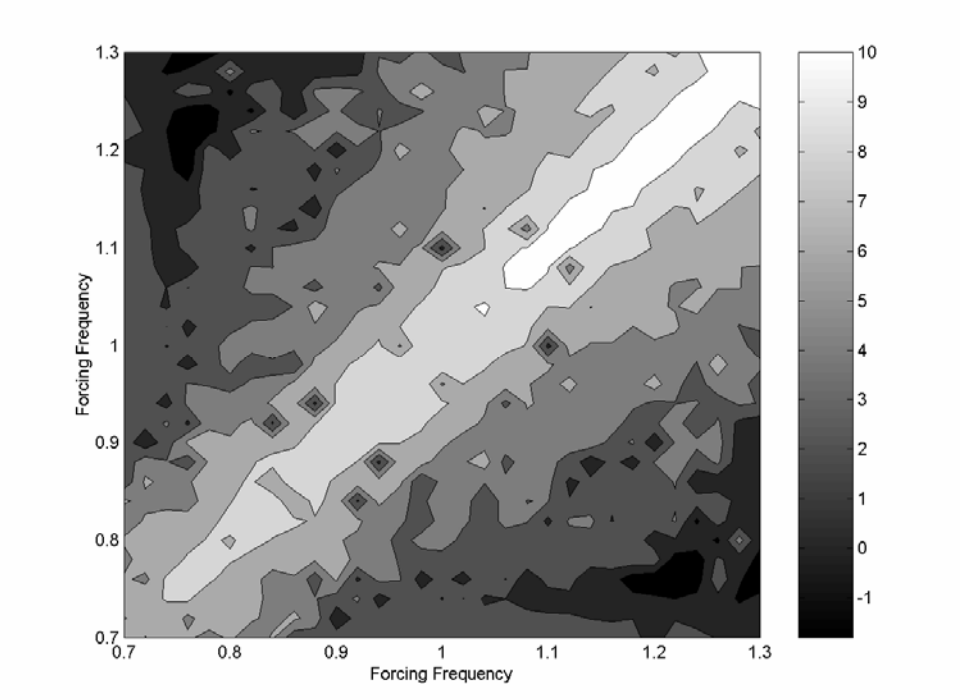

Figure 3.3: Ratio, in dB, of dissipated power of the SSA damper to the base damper

damper and these forcing cases had low relative performance of the SSA. Figure 3.4 shows the ratio of the work extracted by TVA's damper to that of the base damper for the same range of excitation frequencies. As can be seen, for about half of the forcing cases, the TVA's absorber dissipates less power than that of the base damper. The ratio values cross from positive to negative at the same frequencies where the SSA begins to improve its performance relative to a TVA as seen in Figure 3.1. Also, the excitation combination that results in the lowest absorber damper to base damper power dissipation ratio was the same as the excitation resulting in best relative performance of the SSA. In general, an absorber's performance improves when the absorber's damper dissipates more energy than the base damper. Since state switching has little effect on the power input to a system and all this input power must be dissipated by the system's dampers, maximizing

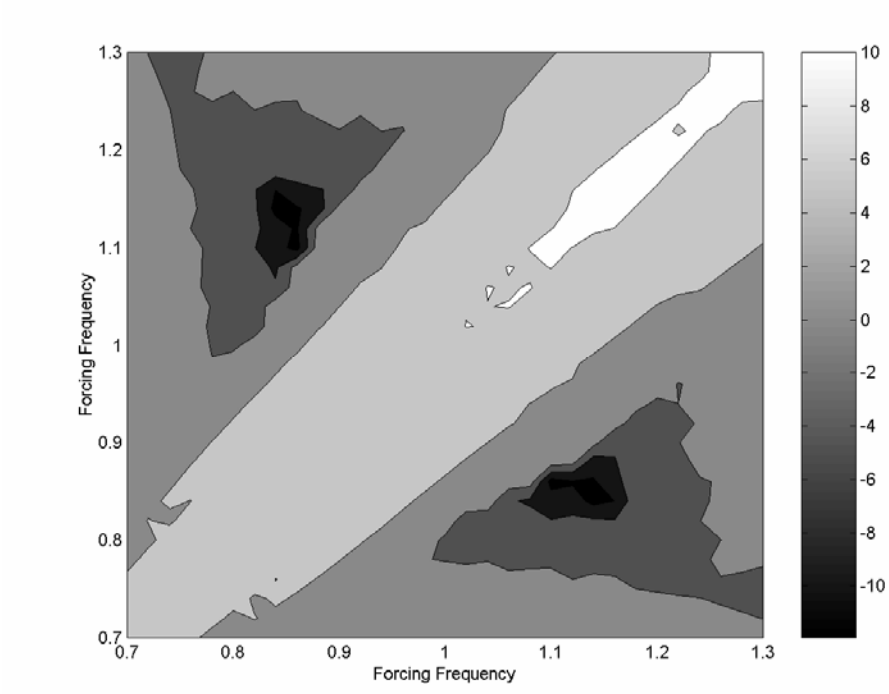

Figure 3.4: Ratio, in dB, of dissipated power of the TVA damper to the base damper

the work extracted by the SSA's damper leads reduced motion in the base to which the absorber is attached.

STABILITY

Kurdila et al. [37] have researched the stability of state-switched systems. They showed that certain switching rules can induce instabilities in systems. The following is a brief summary of Kurdila el al.'s [37] research outlining a switching example that leads to instabilities in the system. That example will be followed by a stability investigation of the switching rule defined by Equations (2.2) and (2.3) used for the research at hand.

Consider a two-state stiffness switching system with no damping. Such a system has two potential "on-line" states defined by

$$\begin{aligned} m\ddot{x} + k_1 x &= 0 \\ m\ddot{x} + k_2 x &= 0 \end{aligned}, \tag{3.1}$$

where m is mass, x is displacement, and k_1 and k_2 are the lower and upper stiffnesses, respectively. Since energy is conserved in Equation (3.1) for any initial condition,

$$\begin{aligned} \frac{1}{2} m\dot{x}^2 + \frac{1}{2} k_1 x^2 &= E_1 \\ \frac{1}{2} m\dot{x}^2 + \frac{1}{2} k_2 x^2 &= E_2 \end{aligned}, \tag{3.2}$$

where E_1 and E_2 are mechanical energies of the lower and upper stiffness states, respectively. Equation (3.2) is an ellipse phase space represented by

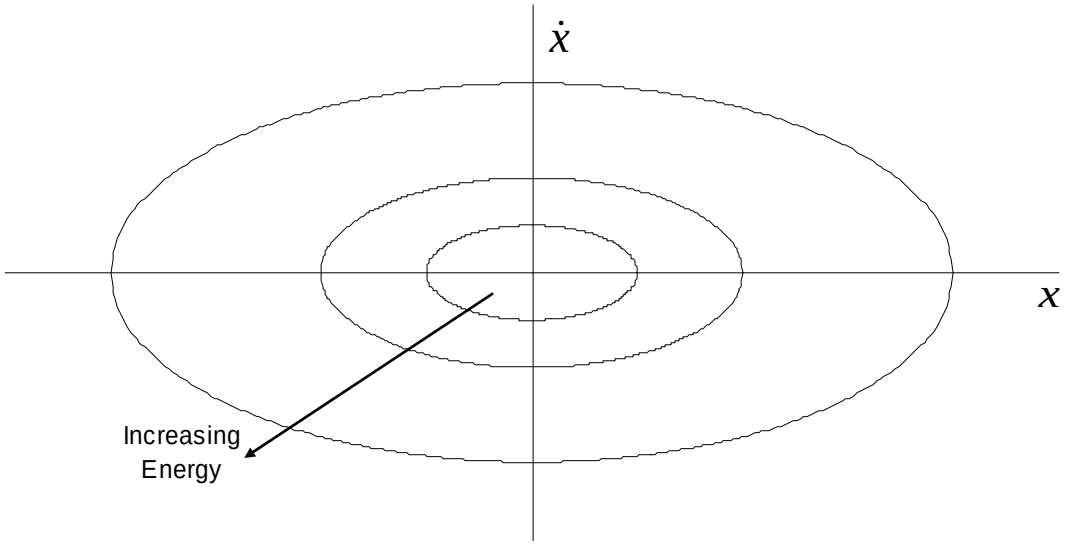

Figure 3.5: Phase portrait of a single stiffness state

$$\begin{aligned} \frac{m}{2E_1}\dot{x}^2 + \frac{k_1}{2E_1}x^2 &= 1 \\ \frac{m}{2E_2}\dot{x}^2 + \frac{k_2}{2E_2}x^2 &= 1 \end{aligned} \quad . \tag{3.3}$$

Figure 3.5 depicts a graphical representation of several energy ellipses of one of the stiffness states defined in Equation (3.3). The larger the ellipse in the phase portrait depicted in Figure 3.5, the more energy the system contains. If a response trajectory plotted on a phase portrait is bounded, the system energy remains bounded and finite, therefore the system is determined to be stable.

Figure 3.6 shows a switching rule that leads to the trajectory shown in Figure 3.7. The switching rule states that if the displacement and velocity are in the same direction, the absorber should be in the lower stiffness state; otherwise, the absorber should be tuned to the upper stiffness. Such a switching rule will switch each time the trajectory crosses an axis. It can be seen from Figure 3.7 that the trajectory moves to a higher

energy ellipse with every switch representing an unbounded, therefore unstable, trajectory. An external energy source is required to complete each switch and move to a higher energy state. Figure 3.7 demonstrates that an unstable system can result from

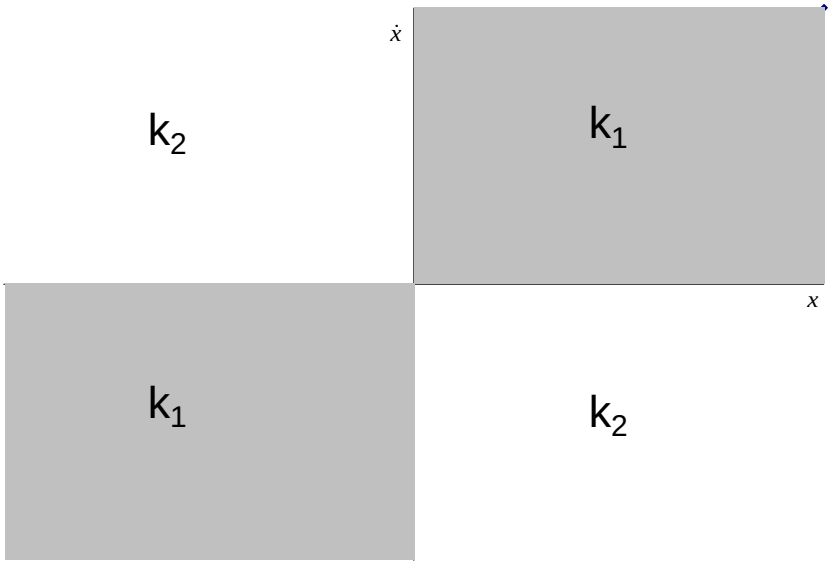

Figure 3.6: Switching rule for unstable example

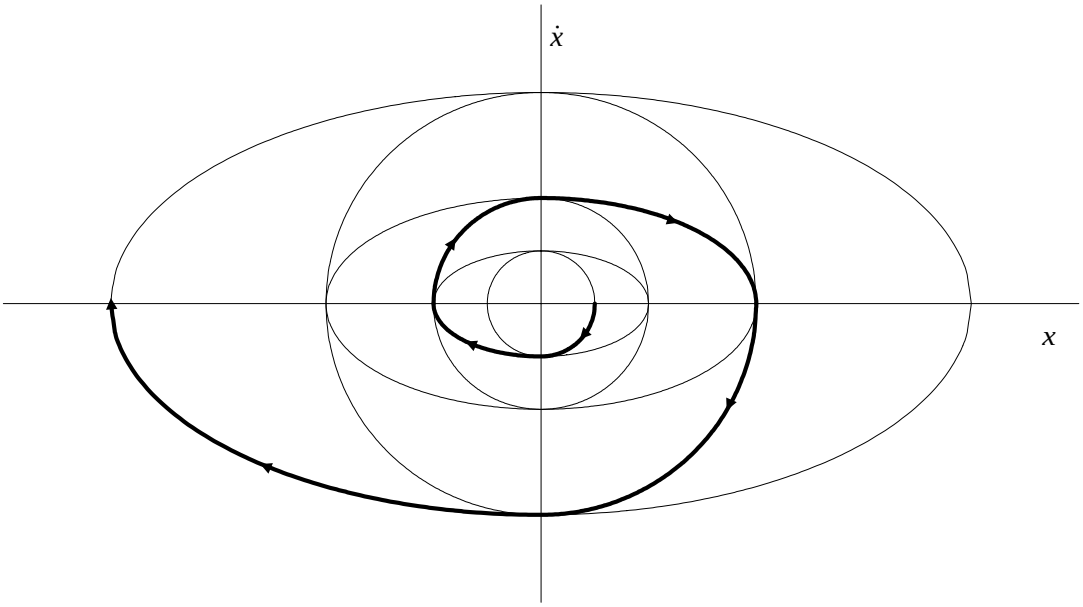

Figure 3.7: Trajectory of an unstable switched system

certain switching rules, even though each state is, itself, neutrally stable.

Kurdila et al.'s [37] example, outlined above, showed that a switched system could become unstable for certain switching rules. A similar approach is taken to show that the switching rule defined in Equations (2.2) and (2.3) is stable. Equations (3.1) and (3.2) defining the equations of motion and energy conservation are identical for switching rule at hand. Figure 3.8 shows the energy trajectories for the two states of the system. Equation (2.2) states that switches may only occur at zero displacement across the spring of the absorber. Therefore, switching may only occur when the trajectory crosses the vertical axis. Because of this zero displacement switch criteria, the system switches between only two energy trajectories and thus is bounded. The switching rule as used in this research is stable, as the energy remains bounded regardless of the number of switches.

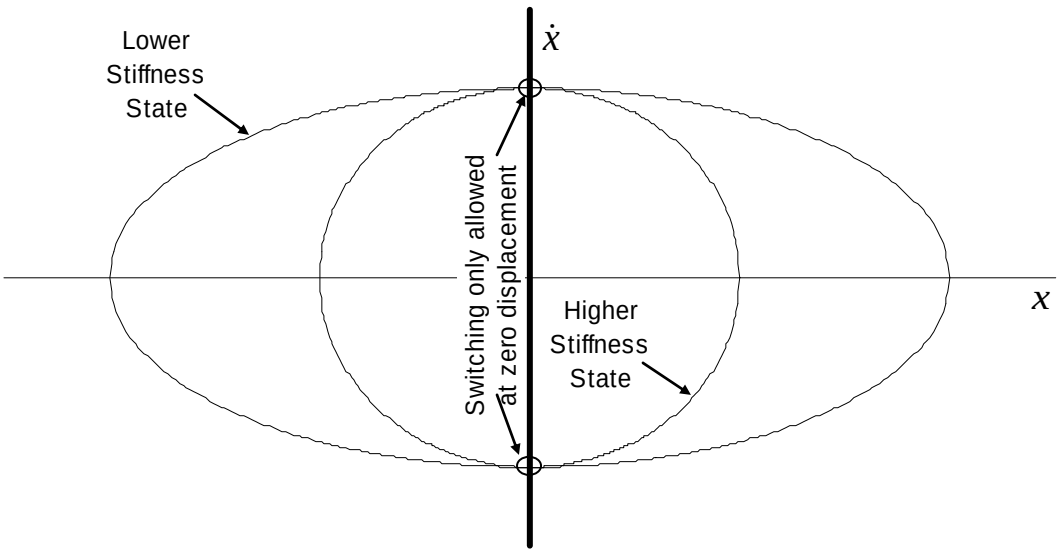

Figure 3.8: Phase portrait of maximum work extraction switching rule

SWITCH TIMING

Real state switching systems have sensors and electronics that are real devices with finite response time. Because of this, switches in real systems cannot occur instantaneously. This non-instantaneous switch can affect the performance of a state-switched absorber used for vibration control. The following sections detail the effect the timing of switch events has on the performance of the state-switched absorber used for vibration control. The first section considers a delay in an instantaneous switch event. The following section details the effect of a switch event that occurs over some finite time.

Delayed Switched

Ideally, switch events occur when the relative displacement equals zero, therefore there is no change in the potential or kinetic energy and the response of the system is continuous across the switch event. However, in real systems, switch events cannot occur exactly at zero displacement. If a switch occurs at a nonzero displacement, one of two things will happen. In one situation, a discontinuous velocity response allows the energy to be conversed. If energy cannot be conserved, energy must be added to the system from an external source to complete the switch. If energy is added to the system, instabilities can occur.

Consider the state-switched absorber attached to a moving base considered in the previous section. The energy in such a system is defined by Equation (3.2). In a real system, an instantaneous change in displacement cannot physically occur. Therefore, a step in the displacement response of the system is not allowed. However, an

instantaneous change in velocity is allowed. If a switch from high stiffness to low stiffness occurs at some relative displacement other than zero, the potential energy instantaneously decreases, as the displacement remains constant across the switch. To conserve energy, the kinetic energy must increase an amount equal to the loss of potential energy. An instantaneous change in velocity occurs to conserve energy across the switch. Now consider a switch from low stiffness to high stiffness at a nonzero relative displacement. The potential energy increases, causing a decrease in kinetic energy. Since the kinetic energy cannot decrease below zero, there are cases where the kinetic energy cannot be decreased enough to conserve energy. In such cases, energy must be added to the system to complete the switch. The addition of energy can cause the state-switched absorber system to become unstable.

Figure 3.9 depicts the phase portrait of an undamped state-switched absorber attached to moving base where switching is delayed. The energy ellipses of the same color in Figure 3.9 represent energy paths that have equivalent energies. From the defined switching rule, switches should occur when the trajectory crosses the vertical axis. However, for the case at hand switch events are delayed by a constant time interval after the zero displacement crossing. The system starts in the upper stiffness state. When the first delayed switch event occurs, the systems instantaneously jumps to the lower stiffness state path of the energy. This occurs with no change in displacement resulting in a vertical trajectory in Figure 3.9 representing a step change in the velocity response. At the next delayed switch event, the system moves from the lower stiffness to the upper stiffness. The system again attempts to jump to the equivalent energy path of the upper state by removing kinetic energy. However, the velocity reaches zero before the

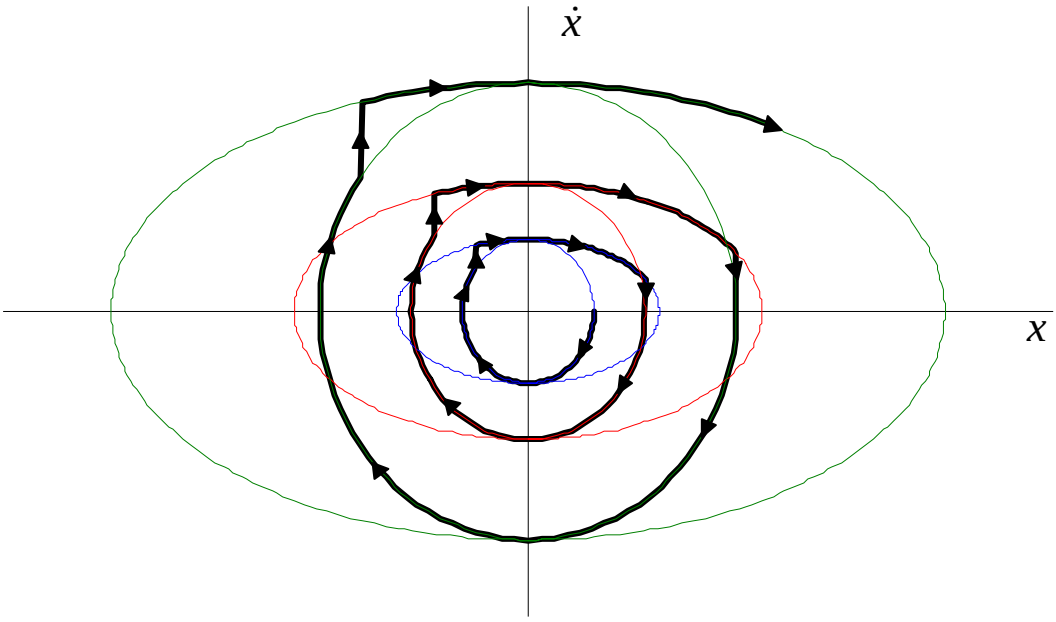

Figure 3.9: Phase portrait of a state switching system with a delayed instantaneous switch

trajectory reaches the upper stiffness state of the same energy. To complete the switch, energy must be added to the system causing the trajectory to follow a higher energy path. As delayed switches continue, the energy continues to increase and the system diverges becoming unstable.

A state-switched system can become unstable when the kinetic energy cannot be reduced enough to balance the energy conservation and energy must be added. As shown in Figure 3.9, a switch event must occur before the displacement in the lower stiffness trajectory is greater than the maximum displacement in the upper stiffness path with the same energy to avoid instabilities. To quantify this statement, consider the total energy in the system when the velocity is zero, or when there is only potential energy in the spring,

$$E_1 = \frac{1}{2} k_1 X_1^2$$
$$E_2 = \frac{1}{2} k_2 X_2^2 \,. \tag{3.4}$$

X is the displacement amplitude, k is the stiffness, and the subscripts *1* and *2* correspond to the lower and upper stiffness states, respectively. By equating the energies defined in Equation (3.4), a relationship between the displacement amplitudes of the two states of equal energy is determined by

$$X_1 = \sqrt{\frac{k_2}{k_1}} X_2 = \frac{\omega_2}{\omega_1} X_2 \,. \tag{3.5}$$

where ω is the natural frequency of the absorber. The displacement response of the SSA in its lower state is of the form

$$x_1 = X_1 \sin(\omega_1 t) \,. \tag{3.6}$$

The latest a switch can occur is the displacement in the lower state equals the displacement amplitude of the upper state, thus keeping the total energy constant across the switch. Equating the lower state's displacement defined in Equation (3.6) with the displacement amplitude of the upper state results in

$$X_2 = \frac{\omega_2}{\omega_1} X_2 \sin(\omega_1 t) \,. \tag{3.7}$$

Simplifying Equation (3.7) gives

$$\Delta t = \frac{1}{\omega_1} \sin^{-1}\left(\frac{\omega_1}{\omega_2}\right). \tag{3.8}$$

Equation (3.8) defines the maximum time delay, Δt, in switching before the state-switched absorber system has the potential to become unstable. This maximum time delay is frequency dependent as can be calculated from knowledge the SSA tuning frequencies.

Ramped Switch

Another type of switch that can cause imprecise timing of switch events is a ramped switched. A ramped switch is one where the switch does not occur instantaneously; it gradually moves from one stiffness to another over some finite time. Many state switching implementations, such as piezoelectrics and magneto-rheological elastomers, do not allow for instantaneous switching. For example, piezoelectrics require the electric charge to build up in order switch. This charge does not appear and disappear instantaneously. The charge is ramped up and down, thus causing the stiffness to also ramp up and down during switch events. The work at hand considers a stiffness switch that changes between states linearly as a function of time. The stiffness change is defined as

$$k = k_- + \frac{t}{T}\left(k_+ - k_-\right) \quad 0 \le t \le T \tag{3.9}$$

where k is the stiffness, t is time, T is the duration of the switch, and the subscripts – and + represent the initial and final state of the switch, respectively.

The phase portrait of a state switching system with ramped switching is shown in Figure 3.10. The system starts in the upper stiffness state and begins its ramped switched

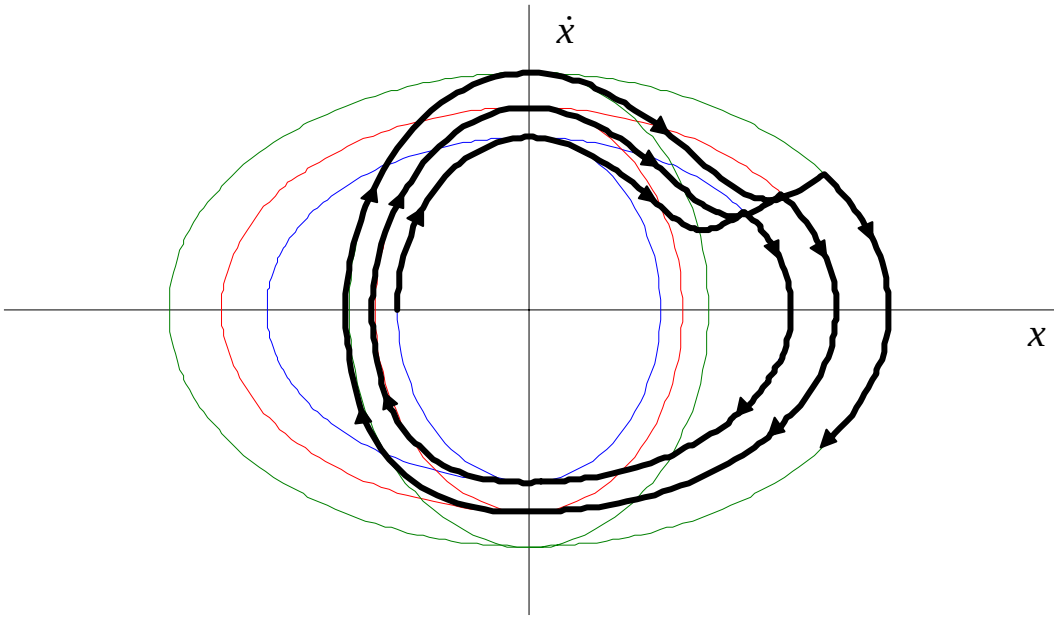

Figure 3.10: Phase portrait of state switching system with ramped stiffness switch

to the lower state once its trajectory reaches zero relative displacement. At this point, the stiffness is linearly decreased as a function of time until it reaches the lower stiffness. As with the delayed instantaneous switch, the system can always conserve energy by increasing the kinetic energy and not adding external energy. Conversely, when the system switches from the lower stiffness to the higher stiffness, the stiffness is gradually increased to the higher state. As this occurs, the potential energy steadily increases while the kinetic energy steadily decreases. If the system reaches zero velocity, or zero kinetic energy, the kinetic energy cannot be reduced any more. For this case, external energy must be added to the system to achieve the stiffness change. This energy is gradually added until the switch is complete, at which point the system's trajectory is at a higher energy level. As this response continues, energy is added with each switch from low

stiffness to high stiffness causing the trajectory to diverge and the system to become unstable.

CHAPTER 4

EQUATIONS OF MOTION

This chapter derives the governing equations of motions for the state-switched absorber systems considered in this research. The following development was used in optimizing the tuning parameters of the SSA used for vibration control. First, a cantilever beam with an absorber attached is outlined. The last section details the equations of a state-switched absorber applied to a plate clamped on all sides.

CANTILIEVER BEAM

Figure 4.1 depicts a state-switched absorber used to control a vibrating beam. The equations of motion for such a system are of the form

$$M\ddot{q} + C\dot{q} + K_s q = U \tag{4.1}$$

where M is the mass matrix, C is the damping matrix, U is a vector of forces, q is a vector of coordinates, and K_s is the stiffness matrix where the subscript s represents the current

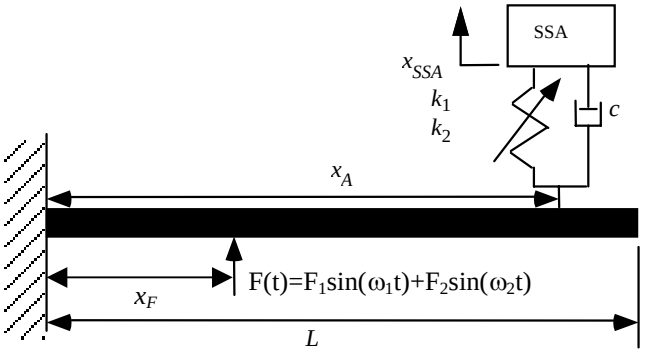

Figure 4.1: State-Switched absorber attached to a beam, subject to multi-harmonic point forcing

state of the SSA.

The method of assumed modes is used to derive the equations of motion.[42] The flexural displacement field on the beam is represented as

$$w(x,t) = \sum_{i=1}^{N} \varphi_i(x) q_i(t) = \varphi^T q \,, \tag{4.2}$$

where N is the number of modes in the isolated beam, φ are basis functions, x is position along the beam, and q is a vector of generalized coordinates. For simplicity x and t will be omitted henceforth.

The kinetic energy for the beam and attached absorbers is

$$T = \frac{1}{2}\int_0^L m(x)\,\dot{w}^2 dx + \frac{1}{2}\sum_{a=N+1}^{N+NA} m_a \dot{q}_a^2 \,, \tag{4.3}$$

where NA is the number of attached absorbers, $m(x)$ is the mass per unit length of the beam and m_a are the masses of the attached absorbers. The elements of the mass matrix, M, are

$$m_{ij} = \begin{cases} \int_0^L m(x)\varphi_i(x)\varphi_j(x)\,dx & i, j \le N \\ m_a & i = j > N \\ 0 & i \ne j > N \end{cases}. \tag{4.4}$$

The potential energy due to the deformation of the beam and springs may be expressed as

$$V = \frac{1}{2}\int_0^L EI(x)\left(\frac{\partial^2 w}{\partial x^2}\right)^2 dx + \frac{1}{2}\sum_{a=N+1}^{N+NA} k_a\left(q_a - w(x_a)\right)^2 \tag{4.5}$$

where E is the modulus of elasticity, I is the area moment of inertia, x_a are the absorber locations, and k_a are the absorbers' stiffnesses. The elements of the stiffness matrix, K, are

$$k_{ij} = \begin{cases} \int_0^L EI(x)\frac{\partial^2\varphi_i(x)}{\partial x^2}\frac{\partial^2\varphi_j(x)}{\partial x^2}dx + \sum_{a=N+1}^{N+NA} k_a\varphi_i(x_a)\varphi_j(x_a) & i, j \le N \\ -k_a\varphi_i(x_a) & i \le N,\ j > N \\ -k_a\varphi_j(x_a) & j \le N, i > N \\ k_a & i = j > N \\ 0 & i, j > N \ \&\ i \ne j \end{cases}, \tag{4.6}$$

There are two discrete K matrices as there are two allowable stiffness states in the state-switched absorbers attached to the beam. Note that each state-switched absorber attached to the beam has two discrete stiffnesses that can be observed depending on what the "on-line" state is.

The work at hand specifically considers the cantilever beam system depicted in Figure 4.1. To satisfy the geometric boundary conditions of displacement and slope equaling zero at x=0, the basis functions are assumed to be

$$\varphi_i(x) = \left(\frac{x}{L}\right)^{i+1}, \tag{4.7}$$

For the work at hand, only one absorber is attached to the beam, which has a mass that is one-tenth the total mass of the beam ($m_a = \rho AL/10$). Assuming the beam has a constant mass per unit length, m_L, the elements of the mass matrix become

$$m_{ij} = \begin{cases} \dfrac{m_L L}{i+j+3} & i, j \le N \\ m_a & i = j > N \\ 0 & i \ne j > N \end{cases}. \tag{4.8}$$

Assuming *EI(x)* is constant along the length of the beam, the elements of the stiffness matrix become

$$k_{ij} = \begin{cases} \dfrac{EIij(i+1)(j+1)}{(i+j-1)L^3} + k_{SSA}\left(\dfrac{x_A}{L}\right)^{i+1}\left(\dfrac{x_A}{L}\right)^{j+1} & i, j \le N \\ -k_{SSA}\left(\dfrac{x_A}{L}\right)^{j+1} & i \le N, j = N+1 \\ -k_{SSA}\left(\dfrac{x_A}{L}\right)^{i+1} & j \le N, i = N+1 \\ k_i & i = j = N+1 \end{cases}. \tag{4.9}$$

The work at hand assumes a two-harmonic point force located at the midpoint along the length of the beam, $x_F = L/2$, giving a forcing vector of

$$U_i = F\varphi_i\left(\frac{L}{2}\right). \tag{4.10}$$

Proportional damping is used to model the damping in this system. The damping matrix is defined as

$$C = \alpha\left(M + K_{avg}\right), \tag{4.11}$$

where α is a proportionality constant and K_{avg} is the mean of the two SSA stiffness matrices. For the work at hand, the proportionality constant is equal to 0.05. An average of the two SSA stiffness matrices is used in Equation (4.11) because the stiffness matrix

can change during the response of the system and a switch in stiffness would cause damping switching, which is not the focus of the research.

CLAMPED PLATE

Figure 4.2 depicts a rectangular plate clamped on all sides with a state-switched absorber attached to control vibrations. The equations of motion for a plate are of the same form as a beam defined by Equation (4.1). As with the beam system, the method of assumed modes is used to model the plate system. The flexural displacement field of the plate is represented as

$$w(x,y,t)=\sum_{i=1}^{N}\varphi_i(x,y)q_i(t)=\varphi^T q\,, \tag{4.12}$$

where x and y define position on the plate. Position and time dependency notation will be dropped henceforth for simplicity.

The kinetic energy of the plate with absorbers attached is expressed as

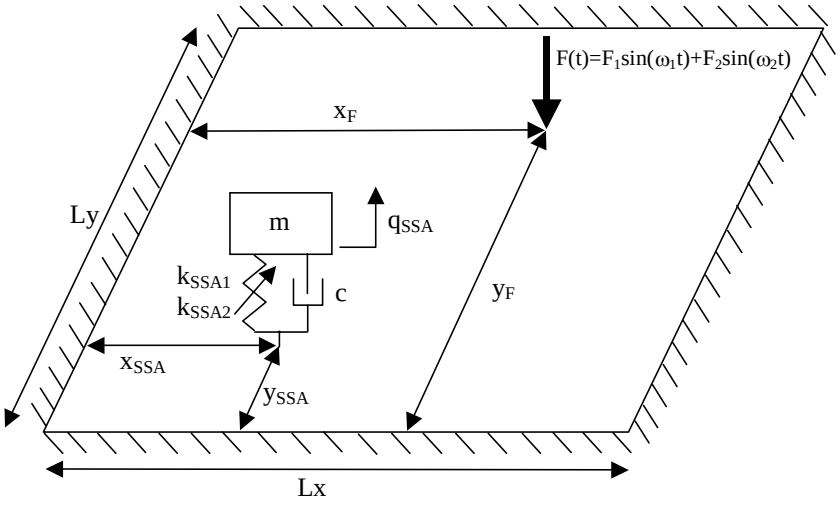

Figure 4.2: State-switched absorber attached to a plate, subject to multi-harmonic point forcing

$$T = \frac{1}{2}\int_0^{L_x}\int_0^{L_y} m(x,y)\dot{w}^2(x,y)dydx + \frac{1}{2}\sum_{a=N+1}^{N+NA} m_a \dot{q}_a^2 \ . \tag{4.13}$$

The elements of the mass matrix are

$$m_{ij} = \begin{cases} \int_0^{L_x}\int_0^{L_y} m\varphi_i\varphi_j dydx & i,j \le N \\ m_a & i,j > N \\ 0 & i \ne j > N \end{cases} . \tag{4.14}$$

As with the beam system, the absorber mass is one-tenth the mass of the plate. The potential energy for the plate and attached absorbers may be expressed as [43]

$$V = \frac{1}{2}\int_0^{L_x}\int_0^{L_y} D(x,y)\left\{w_{xx}^2 + w_{yy}^2 + 2\nu w_{xx}w_{yy} + 2(1-\nu)w_{xy}^2\right\}dydx + \frac{1}{2}\sum_{a=N+1}^{N+NA} k_a\left(q_a - w(x_a,y_a)\right)^2 \tag{4.15}$$

where

$$D(x,y) = \frac{E(x,y)h(x,y)^3}{12\left(1-\nu^2\right)}, \tag{4.16}$$

h is the plate thickness, ν is Poisson's ratio, and x_a and y_a define the absorber's position on the plate. The elements of the stiffness matrix are calculated similarly to that of the beam and are

$$k_{ij} = \begin{cases} \int_0^{L_x}\int_0^{L_y} L(\varphi_i,\varphi_j)dydx + \sum_{a=N+1}^{N+NA} k_a\varphi_i(x_a,y_a)\varphi_j(x_a,y_a) & i,j \le N \\ -k_a\varphi_i(x_a,y_a) & i \le N, j > N \\ -k_a\varphi_j(x_a,y_a) & j \le N, i > N \\ k_a & i = j > N \\ 0 & i,j > N \ \& \ i \ne j \end{cases} \tag{4.17}$$

where

$$L(\varphi_i, \varphi_j) = D(\varphi_{xx,i}\varphi_{xx,j} + \varphi_{yy,i}\varphi_{yy,j} + 2\nu\varphi_{xx,i}\varphi_{yy,j} + 2(1-\nu)\varphi_{xy,i}\varphi_{xy,j}). \tag{4.18}$$

As with the beam system, there are two discrete stiffness matrices representing each of the two potential stiffnesses between which the absorber can switch.

The research at hand considers a square plate that has been clamped on all four sides. The basis function used to satisfy the boundary conditions of such a plate is

$$\varphi_i(x,y) = \frac{x}{L_x}\left(1-\frac{x}{L_x}\right)\sin\left(\frac{m\pi x}{L_x}\right)\frac{y}{L_y}\left(1-\frac{y}{L_y}\right)\sin\left(\frac{n\pi y}{L_y}\right), \tag{4.19}$$

where m and n are integer indices mapping to the subscript i. The number of degrees of freedom in the plate is determined by the maximum values of m and n,

$$DOF_{plate} = m \times n. \tag{4.20}$$

The elements of the mass matrix for a clamped plate become

$$m_{ij} = \begin{cases} \rho h \int_0^{L_x}\int_0^{L_y}\left(\frac{x}{L_x}\left(1-\frac{x}{L_x}\right)\frac{y}{L_y}\left(1-\frac{y}{L_y}\right)\right)^2 \sin\left(\frac{m\pi x}{L_x}\right)\sin\left(\frac{n\pi y}{L_y}\right)\sin\left(\frac{r\pi x}{L_x}\right)\sin\left(\frac{s\pi y}{L_y}\right)dydx & i, j \le DOF_{plate} \\ m_a & i, j > DOF_{plate} \\ 0 & i \ne j > DOF_{plate} \end{cases} \tag{4.21}$$

where m and n map to the subscript i and r and s map to the subscript j. The elements of the stiffness matrix are

$$k_{ij} = \begin{cases} \int_0^{L_x}\int_0^{L_y} L(\varphi_i,\varphi_j)dydx + k_a\left(\frac{x_a}{L_x}\left(1-\frac{x_a}{L_x}\right)\frac{y_a}{L_y}\left(1-\frac{y_a}{L_y}\right)\right)^2 \sin\left(\frac{m\pi x_a}{L_x}\right)\sin\left(\frac{n\pi y_a}{L_y}\right)\sin\left(\frac{r\pi x_a}{L_x}\right)\sin\left(\frac{s\pi y_a}{L_y}\right) & i, j \le DOF_{plate} \\ -k_a\frac{x_a}{L_x}\left(1-\frac{x_a}{L_x}\right)\sin\left(\frac{m\pi x_a}{L_x}\right)\frac{y_a}{L_y}\left(1-\frac{y_a}{L_y}\right)\sin\left(\frac{n\pi y_a}{L_y}\right) & i \le DOF_{plate}, j > DOF_{plate} \\ -k_a\frac{x_a}{L_x}\left(1-\frac{x_a}{L_x}\right)\sin\left(\frac{r\pi x_a}{L_x}\right)\frac{y_a}{L_y}\left(1-\frac{y_a}{L_y}\right)\sin\left(\frac{s\pi y_a}{L_y}\right) & j \le DOF_{plate}, i > DOF_{plate} \\ k_a & i = j > DOF_{plate} \\ 0 & i, j > DOF_{plate} \;\&\; i \ne j \end{cases} \tag{4.22}$$

As with the mass matrix, m and n map to the subscript i and r and s map to the subscript j. L is calculated using Equation (4.18), again using proper mapping between indices.

The double integrals in Equations (4.21) and (4.22) are calculated numerically using the MATLAB function `dblquad`.

To determine the forcing vector, a point force on the plate located at $x_F = 0.25L_x$ and $y_F = 0.375L_y$ is used. The resulting forcing vector is

$$U_i = F\varphi_i\left(\frac{1}{4}L_x, \frac{3}{8}L_y\right) = \frac{45}{1024}F\sin\left(\frac{\pi m}{4}\right)\sin\left(\frac{3\pi m}{8}\right). \tag{4.23}$$

A damping equivalent to that described in Equation (4.11) is also used in the plate system.

CHAPTER 5

STATE-SWITCHED ABSORBER OPTIMIZATION

This chapter details the optimization of the location and tuning frequencies of the state-switched absorber attached to continuous systems, specifically a beam and plate. The first section describes how the response of the system was modeled and the optimization technique employed. It also explains the objective function and how the performance of an SSA is compared to the performance of a TVA. The final two sections detail the results from the optimization of the beam and plate, respectively.

OPTIMIZATION METHOD

The response of the state-switched absorber system is calculated using a linear time invariant (LTI) state-space method. This method can be used because the system is linear and time invariant between switch events. When a switch event does occur, all the matrices are updated to reflect the new "on-line" state with initial conditions and the LTI simulation continues until the next switch event. Cunefare et al.[40] detailed a more in-depth coverage of this simulation method as it applies to the state-switched absorber.

The goal of this research is to compare the response of an optimized SSA to that of an optimized TVA. The objective function to be optimized is the time averaged kinetic energy of the base system. The kinetic energy of the base system is defined as

$$T = \frac{1}{2}\dot{q}^T M\dot{q}\,, \tag{5.1}$$

where $\dot{q}$ represents the generalized velocities corresponding to the base system and M is the mass matrix corresponding to the base system. The kinetic energy described in Equation (5.1) is averaged over one repetition of the system response. Due to the switching in the system, the SSA can never truly be in steady state. However, a repetition in the response of the system can be observed. This repetition period is the interval over which the kinetic energy is averaged.

There are three or four parameters that can be altered to achieve an optimum performance depending on if the SSA is applied to beam or a plate. One parameter is the location of the absorber's attachment point on the vibrating body. For the beam system, only one value is needed to describe the attachment location, whereas the plate system requires two values to define the absorber placement. The other two parameters are the upper and lower tuning frequencies of the SSA. Note that if the two SSA frequencies are equal, the absorber behaves as a classical tuned vibration absorber. These tuning frequencies, along with the excitation frequencies, are normalized by the natural frequency of the fundamental mode of the base system with no attachment.

Optimization techniques that assume a continuous, but not necessarily convex, objective function to find local maxima and minima cannot be employed for the state switching system. This is due to the discontinuous nature of the kinetic energy objective function as a function of tuning parameters. A slight change in one of the SSA parameters can cause switch events to occur at different instances, which can lead to a significant change in the average kinetic energy of the base system. Due to the discrete

nature of switching, the average kinetic energy objective function changes discontinuously as a function of tuning parameters. Such discontinuities make gradient-based optimizers infeasible, as an infinite slope will cause a failure in the optimization.

To optimize the absorber's attachment location and tuning frequencies, a simulated annealing optimization method was employed. Metropolis et al.[44] developed a simple algorithm that provides an efficient simulation of the annealing process of materials. Kirkpatrick et al.[45] recognized that this simulated annealing algorithm could be utilized for optimization problems. Optimization by simulated annealing is beneficial in that it allows for the transition out of local optimum, therefore the procedure need not get stuck in a non-global optimum. However, even though the simulated annealing algorithm allows for movement out of a local optimum, it does not guarantee that a global optimum will be found. For the state-switching problem at hand, simulated annealing is advantageous not only because it won't get stuck in local minimum, but also because it does not require the use of gradients.

The simulated annealing optimization algorithm begins at an initial "temperature" with an initial guess of the optimization parameters corresponding to an objective function value. The procedure randomly selects new parameters in the neighborhood of the previous parameters. These new parameters also each have a corresponding objective function value. If the new value of the objective function is less than the previous objective function value, the move is allowed and the new parameters are accepted as the current parameters, assuming a minimum objective function is desired. If the new value of the objective function is greater than the previous objective function value, the move away from the local minimum is allowed if

$$\exp\left(\frac{f - f_{new}}{c}\right) > random(0,1) \tag{5.2}$$

In Equation (5.2), f is the current objective function value, f_{new} is the objective function value corresponding to the newly determined parameters, c is the simulated annealing temperature, and *random*(0,1) is a number between zero and one chosen using a random number generator. Note that the use of Equation (5.2) allows for movement to a higher objective value, thus the procedure need not get stuck in a local minimum. Whether or not a move occurs, a new set of parameters is chosen in the neighborhood of the current parameters and the process is repeated. After this process has been repeated a predetermined number of iterations at the same "temperature," the "temperature" is lowered a small amount and the steps are repeated at this new "temperature." The algorithm continues until the objective function remains unchanged over a number of consecutive decreasing temperatures. At this point, the system is "frozen" and the optimum is found.

BEAM OPTIMIZATION RESULTS

The simulated annealing optimization algorithm described above was used to optimize the tuning frequencies and the attachment location of the state-switched absorber applied to a vibrating beam. This optimization algorithm was considered for a range of two-frequency component excitations. Each of the two forcing frequencies range from just below the frequency of the beam's first mode to just above the second mode's frequency. There are 16 forcing frequency steps over the range resulting in 136 different forcing combinations. For each combination of forcing frequencies, the simulated annealing algorithm was employed to find the attachment location and tuning

frequencies that resulted in the minimum kinetic energy in the beam. For comparison of the performance of the SSA to classical devices, a similar optimization method was used to optimize the location and frequency of a classical tuned vibration absorber.

Figure 5.1 shows the energy ratio of the optimized state-switched absorber system to a beam with no absorber attached to it. The energy ratio used in Figure 5.1 is calculated by

$$E_r = 10\log\left(\frac{KE_{SSA}}{KE_{beam}}\right), \tag{5.3}$$

where KE_{SSA} is the beam kinetic energy with the optimized SSA attached and KE_{beam} is the kinetic energy of a beam with no absorber attached. When this value is less than zero, a beam with an SSA attached performs better than an untreated beam. The forcing

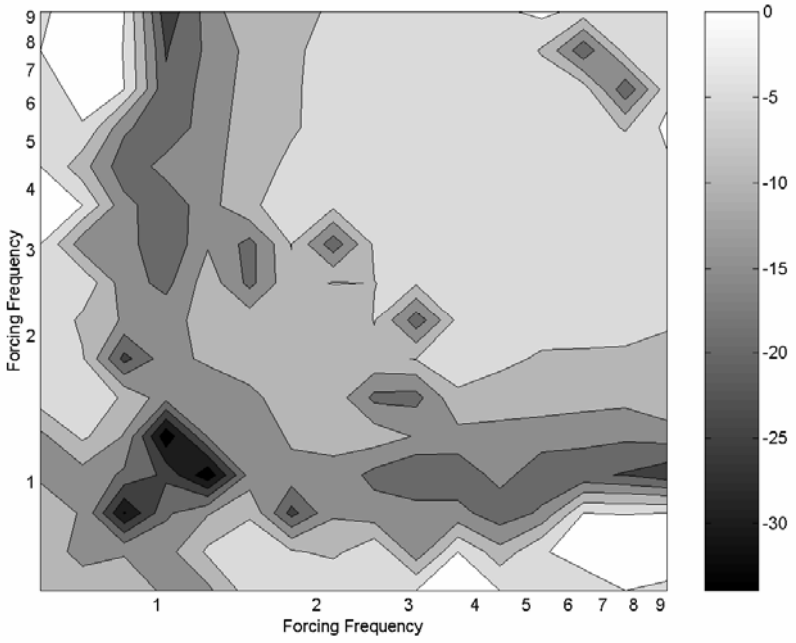

Figure 5.1: Kinetic energy ratio, in dB, of an optimized SSA system to an untreated beam as function of two forcing frequencies

frequencies in Figure 5.1 are all normalized by the frequency of the first mode of the isolated beam. As can be seen from Figure 5.1, the SSA is effective at reducing the vibrations of a vibrating beam for all the forcing cases considered. The best performance of the SSA occurs when the two normalized forcing frequencies are 1.04 and 1.24. The SSA reduces the beam energy by 33.9 dB for this forcing case.

Figure 5.2 shows the energy ratio of the optimized SSA system to the optimized TVA system. All values in Figure 5.2 are determined similarly to that of Figure 5.1. As can be seen from Figure 5.2, an optimized SSA performs as well as or better than an optimized TVA for the entire range of frequencies considered. The best relative performance of the SSA occurred when the normalized forcing frequencies were 6.4 and 7.7 where the SSA reduced the kinetic energy of the beam by 17 dB over that of an

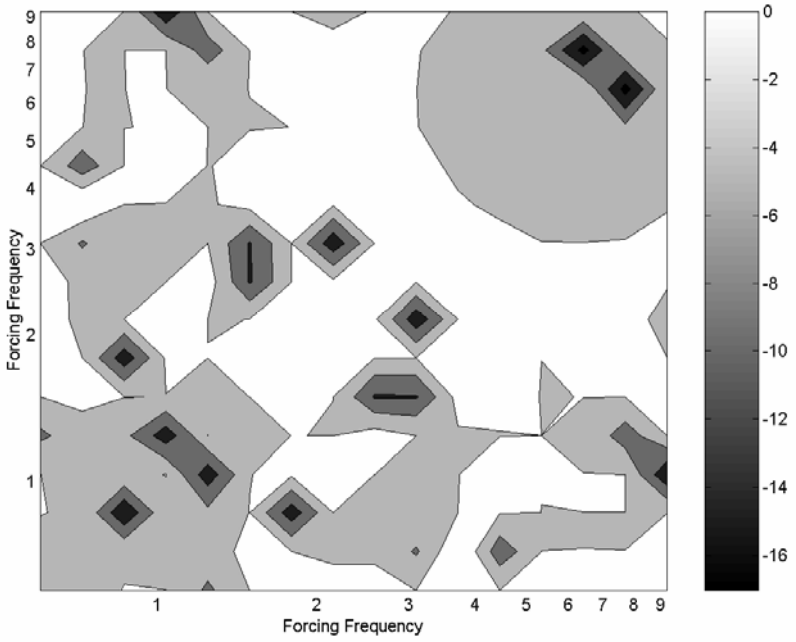

Figure 5.2: Kinetic energy ratio, in dB, of an optimized SSA to an optimized TVA as function of two forcing frequencies

optimized TVA.

Figure 5.3 shows the optimal attachment location of the state-switched absorber along the beam as a function of the two frequency components. The attachment location is normalized by the length of the beam and the forcing frequencies are normalized by the frequency of the first mode of the isolated beam. As can be seen, most of the forcing cases result in an attachment location of one, which corresponds to the free end of the cantilever beam. Over most of the frequency range considered, the first mode of vibration is the mode being controlled. This first mode shape of a cantilever beam has maximum displacement at the free end of the beam, thus the free end vibrates more than any point on the beam. The SSA is placed at the free end to have the greatest effect at controlling the first mode. Figure 5.3 also shows that around the frequency of the second

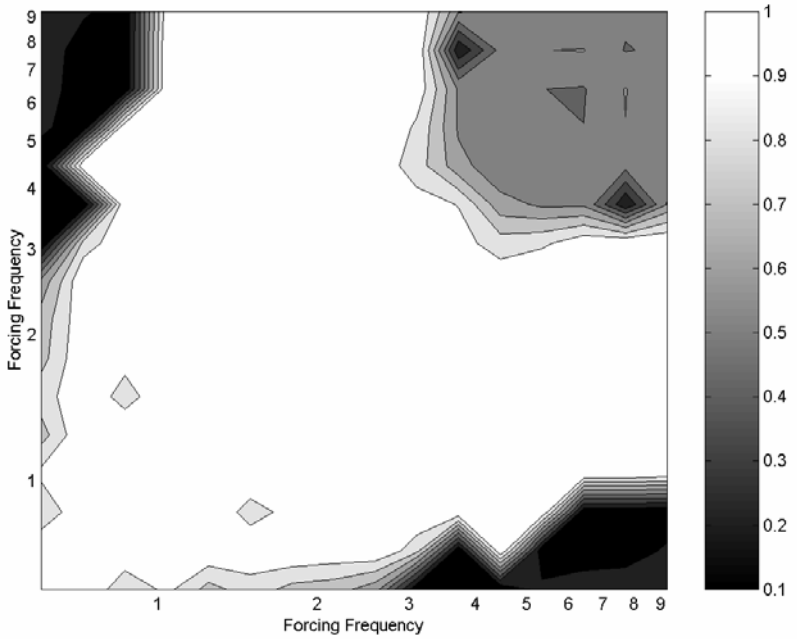

Figure 5.3: Optimum SSA location along a beam as function of two forcing frequencies

mode there is a shift in absorber location. The frequency of the second mode is 6.3 times that of the first mode for a cantilever beam. Also, the largest displacement of the second mode shape occurs near the middle of the cantilever beam. Figure 5.3 shows that the optimum attachment point is near the center of the beam, when the forcing frequencies are near the frequency of the second mode. As with the first mode, the absorber has the greatest effect when attached at the point of greatest vibration.

Figure 5.4 plots the average of the two optimized state-switched absorber frequencies versus each of the two forcing frequencies. These average frequencies are normalized by the frequency of the first mode of the isolated beam. As can be seen from Figure 5.4, as the forcing frequencies increase the average tuning frequency also increases. This result is as expected since the tuning frequencies should be tuned near the

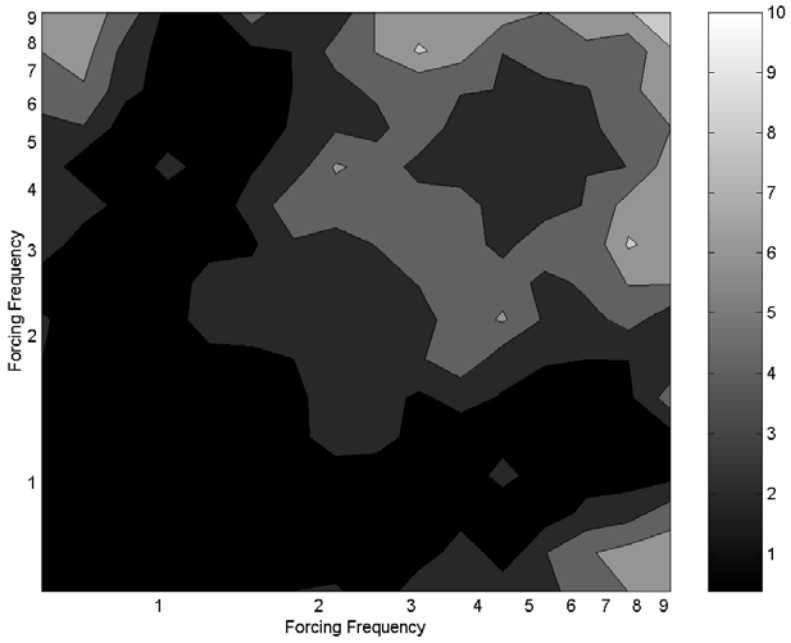

Figure 5.4: Mean of two SSA tuning frequencies normalized by first mode of beam as function of two forcing frequencies

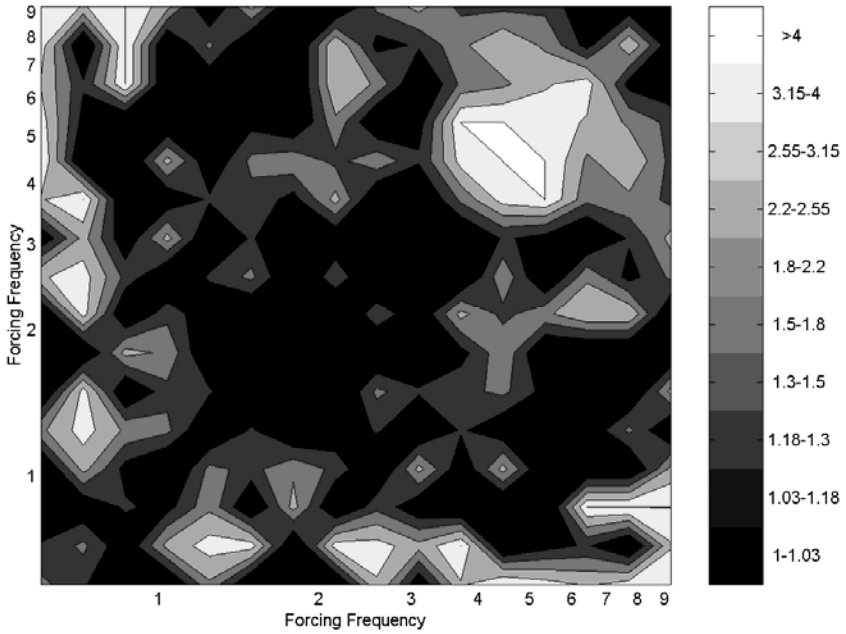

Figure 5.5: Ratio of optimum SSA tuning frequencies as function of two forcing frequencies

excitation frequencies the SSA is trying to control. Figure 5.5 depicts the ratio of the two optimized state-switched absorber tuning frequencies as a function of the two forcing frequency components. When this ratio is one, the two SSA frequencies are equal and the absorber acts similarly to a classical tuned vibration absorber. As the ratio increases, the spacing between SSA frequencies also increases. When Figure 5.5 is compared to Figure 5.1, it can be seen that the forcing combinations that result in a frequency ratio of one closely correlate to the forcing cases that result in an SSA/TVA energy ratio equaling zero dB. At these forcing cases, the simulated annealing algorithm is choosing the SSA frequencies to be equal, thus choosing a TVA. When the optimization was repeated for the TVA, it chose the exact same absorber as was found by the SSA optimization resulting in equal beam kinetic energies. In other words, the optimization found the best SSA to be a TVA for these forcing cases. Also, Figure 5.5 shows that a large spacing in

available tuning frequencies does not necessarily result in improved performance of the SSA over a TVA. The cases that resulted in the best relative performance of the SSA all had frequency ratio of less than two. MR elastomers have a potential tuning frequency ratio of 4.[46] Therefore, the frequency shifts necessary to achieve maximum performance of the SSA applied to a beam are less than the maximum shift that can be physically realized. This means that an optimal SSA should be able to be fabricated using MR elastomers. Finally, there is no analytical correlation between the forcing frequencies and the optimized tuning frequencies. The combination of Figures 5.4 and 5.5, which defines optimal tuning frequencies, shows no trend in the tuning frequencies as a function of forcing frequencies. Therefore, there is no way to approximate analytically what the optimized tuning frequencies should be based on the forcing frequencies.

The sensitivity of the optimization algorithm must be examined to determine the robustness of the optimization results. The sensitivity is examined by slightly perturbing one of the tuning parameters of the best performing state-switched absorber. As shown in Figure 5.6, the best relative SSA performance occurs when the normalized forcing frequencies are 6.4 and 7.7 and the SSA reduces the kinetic energy 17 dB more than a TVA. The optimized normalized tuning frequencies are 5.07 and 6.11 and the optimal normalized location is 0.6 for this case. To determine the sensitivity of this optimization, teach tuning parameter, including both SSA frequencies, attachment location, and absorber to beam mass ratio, is perturbed within a range of 10% above and below the optimal value while holding all other tuning parameters constant. The ratio of the beam kinetic energy due to the SSA to the kinetic energy of the optimal TVA for this forcing

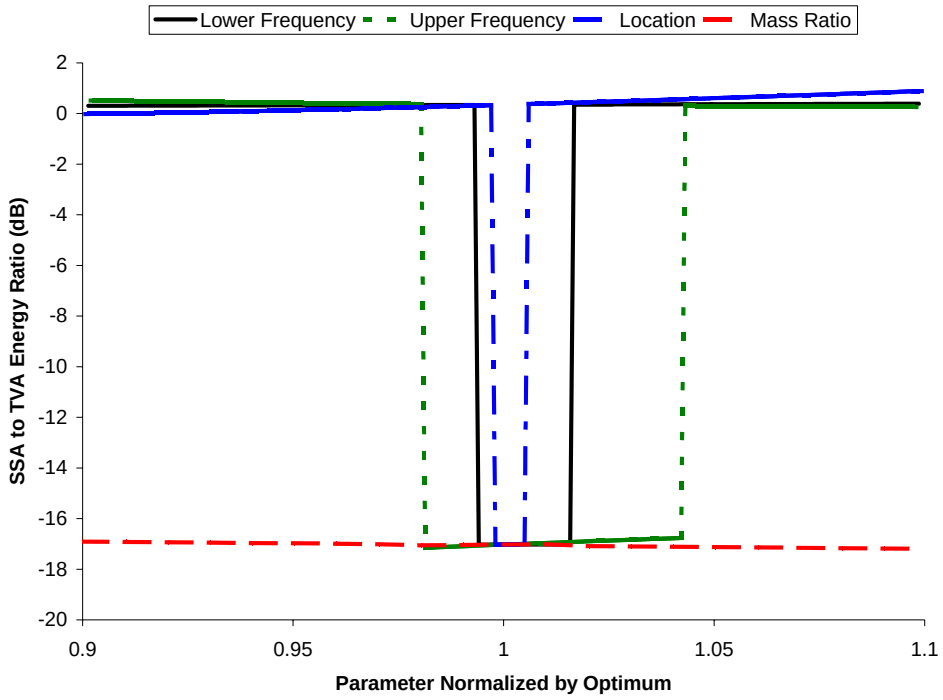

Figure 5.6: Kinetic energy ratio of SSA to optimized TVA as a function of tuning parameters near the best performing SSA

case is shown in Figure 5.6 for the perturbation range. Each tuning parameter is normalized by its optimal value that resulted in the best SSA performance in the optimization. As can be seen, there is about a 17 dB decrease in kinetic energy for a narrow range around each of the optimized frequencies and the attachment location. The bandwidth of the optimal tuning values is about 1% for the attachment location, 2% for the lower tuning frequency, and about 6% for the upper tuning frequencies. This means that perturbing any of these tuning parameters, even by a small amount, can lead to large differences in the performance of the SSA for this specific forcing and tuning case. The simulation results are not sensitive to small perturbations in the mass ratio. As can be seen in Figure 5.6, the beam kinetic energy gradually decreases as the mass ratio

increases. Similar perturbation results can be found from all the sharps peaks seen in Figure 5.2.

The optimization results for the best performing SSA are very sensitive to small perturbations in the tuning parameters. This means that while the tuning parameters yield excellent performance, the likelihood that the optimization finds this narrow range of optimized tuning parameters is very small. Also, when fabricating a physical SSA there may be difficulty in narrowing in on this small band where the SSA performs its best. For certain forcing cases, mistuning the optimal parameters, even by 1%, can cause the SSA to show no performance gains versus a classical TVA.

The sensitivity of the optimization was also investigated for an SSA that performed 0.5 dB better than a TVA, a more typical performance gain found from the optimization than the 17 dB performance gain investigated above. Figure 5.7 shows the SSA to TVA energy ratio for perturbations around the optimal tuning parameters for this "average" performing SSA. All values are normalized and displayed similarly to those in Figure 5.6. Although the results are not as sensitive as the best performing SSAs, the performance of an "average" performing SSA is also sensitive to small perturbations in the tuning frequencies and attachment point. A 4% change in the upper tuning frequency can change the SSA performance by 2.5 dB and a 1% change in attachment location can alter the SSA performance by 0.9 dB. Changes in the lower tuning frequency had very little effect on the SSA performance near this specific optimal tuning case. This "average" SSA's performance is much less sensitive to tuning parameters than that of a high-performance point, where a 1% change in a tuning parameter can change the beam kinetic energy by 17 dB. This means that an SSA designed in this region is more robust

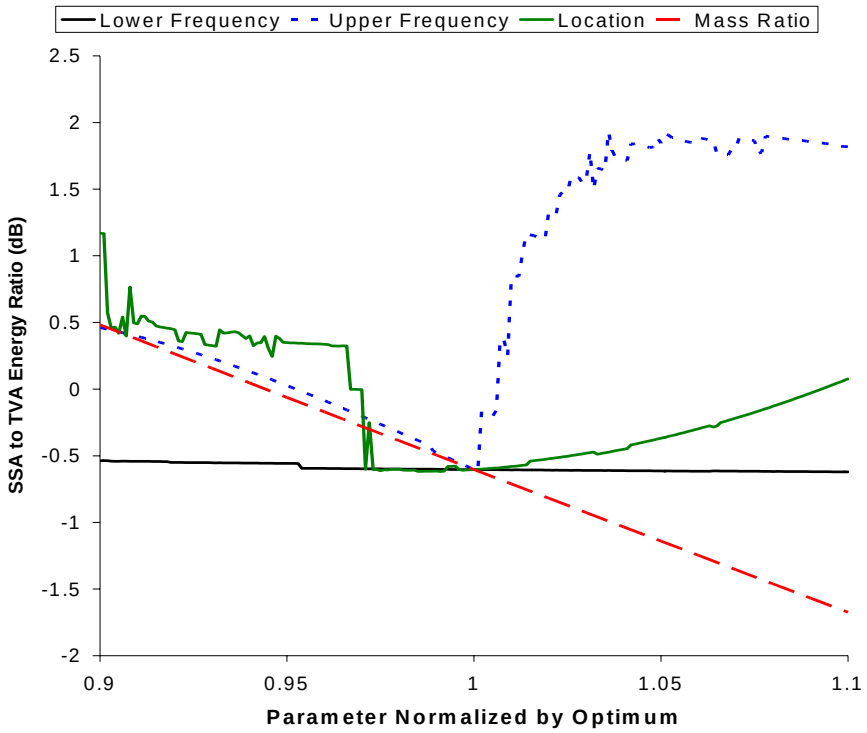

Figure 5.7: Kinetic energy ratio of SSA to optimized TVA as a function of tuning parameters near average performing SSA

than one designed for a high performance region. As with the best performing SSA, the simulation results are not sensitive to perturbations in the mass ratioand the SSA performance improves as the mass ratio increases.

PLATE OPTIMIZATION RESULTS

The simulated annealing optimization algorithm was also used to optimize the tuning frequencies and the attachment location of the state-switched absorber applied to a vibrating plate. A method similar to that used in the beam optimization was employed for the plate optimization. The plate was subjected to a two-frequency component point excitation. Each excitation frequency ranged from just below the natural frequency of the first plate mode to just above the natural frequency of the plate's fifth mode. For each

combination of excitation frequencies, the state-switched absorber's attachment location and tuning frequencies were optimized using the simulated annealing algorithm outlined previously. Note that there are two values that define the attachment location on the two-dimensional plate, whereas the beam system required only one value to define the attachment point. Therefore, there are four parameters to be optimized in the state-switched absorber applied to a plate system. As with the beam system, a similar optimization was done for a tuned vibration absorber to compare the SSA to classical devices.

Figure 5.8 depicts the performance of the state-switched absorber as compared to an untreated plate. The kinetic energy ratio of the SSA system to the untreated system is shown as a function of both forcing frequencies. The energy ratio is quantified on a

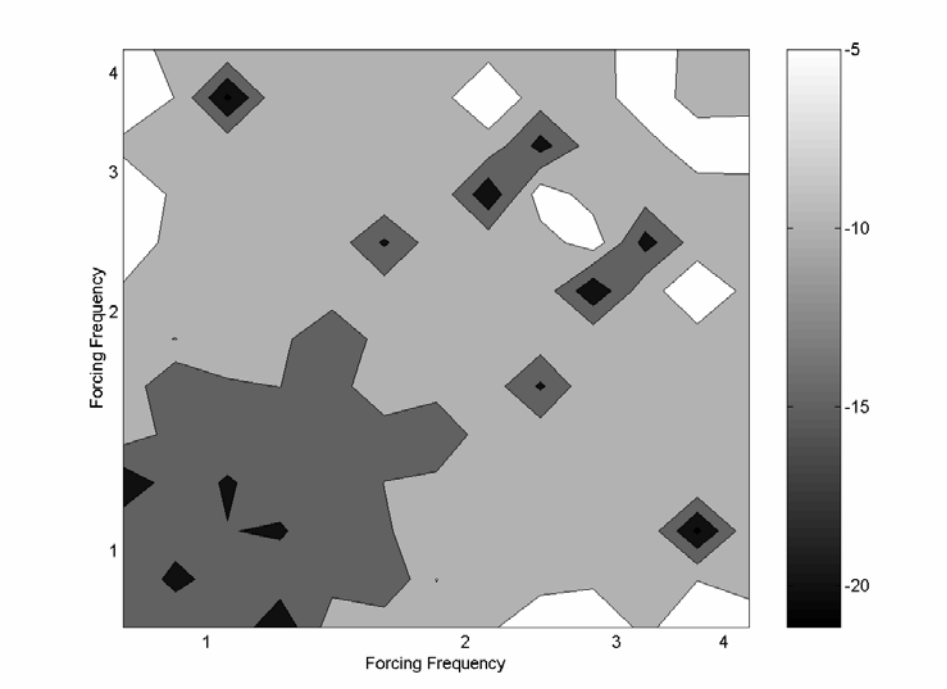

Figure 5.8: Kinetic energy ratio, in dB, of an optimized SSA system to an untreated plate as function of two forcing frequencies

decibel scale as described by Equation (5.3), therefore when the value is less than zero the SSA reduces vibration in the plate. As with the beam, all frequencies have been normalized by the natural frequency of the first mode of the plate. Figure 5.8 shows that the SSA is effective at reducing the vibrations of the plate for the entire range of frequencies considered. The optimized SSA reduced the kinetic energy of the plate the most when the two normalized forcing frequencies were 1.06 and 3.72. For this forcing case, the SSA reduced the kinetic energy of the plate by 21.2 dB.

The relative performance of the optimized state-switched absorber as compared to an optimized tuned vibration absorber is shown in Figure 5.9. The ratio of the plate kinetic energies, in decibels, is plotted as a function of the two forcing frequencies, normalized by the first mode's frequency. For nearly all of the forcing combinations

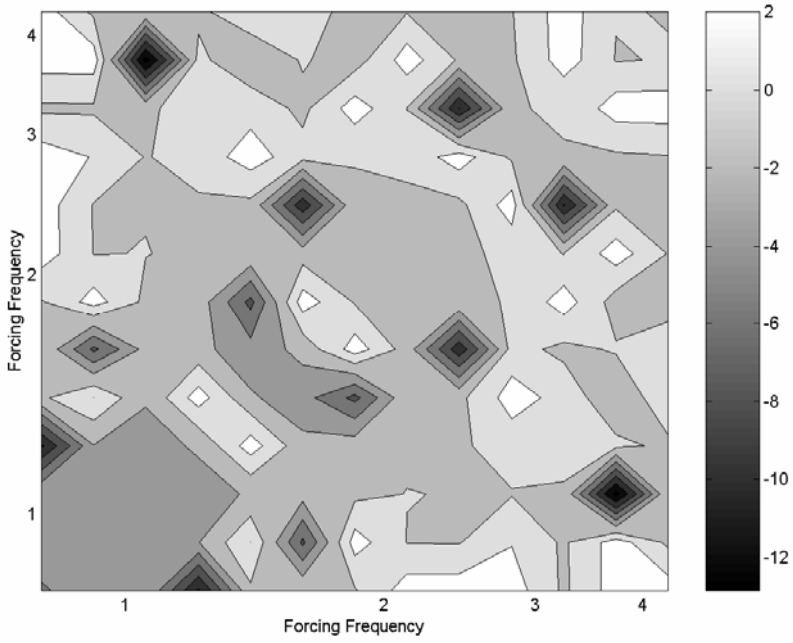

Figure 5.9: Kinetic energy ratio, in dB, of an optimized SSA plate system to an optimized TVA plate system as function of two forcing frequencies

considered, the ratio value is less than zero and the optimized SSA outperforms the optimized TVA. The best relative performance of the SSA occurs when the normalized excitation frequencies are 1.06 and 3.72, where the optimized SSA reduces the plate kinetic energy 12.9 dB more than the optimized TVA does. As with the beam optimization, the sharp peaks seen in Figure 5.9 are strongly sensitive to small perturbations in the tuning parameters. Figure 5.9 also shows that there are forcing frequency combinations where the optimized TVA narrowly outperforms the optimized SSA. For these forcing cases, the simulated annealing algorithm finds a less than optimal local minimum in optimizing the SSA. For these forcing cases, the algorithm could have found both SSA tuning frequencies to be equal to the optimized TVA frequency, thus causing the SSA to act as the optimum TVA. While the simulated annealing algorithm allows for moving out of a local minimum, it does not guarantee that the global minimum will found. So the simulated annealing algorithm can still get stuck in a local minimum, as was the case for a few scattered forcing cases. However, for the vast majority of forcing combinations, the optimized SSA outperformed the optimized TVA. Also, the worst performing SSA only resulted a plate kinetic energy 2 dB more than an optimized TVA, whereas the best performing SSA resulted in a plate kinetic energy 12.9 dB less than an optimized TVA.

Figures 5.10 and 5.11 define the attachment point of the optimized state-switched absorber on the plate for the range of two-frequency excitations considered. Since the plate has two dimensions, two values are required to define the attachment location on the plate. The locations defined by Figures 5.10 and 5.11 are normalized by the length of the plate in the respective directions and the frequencies are normalized by the natural

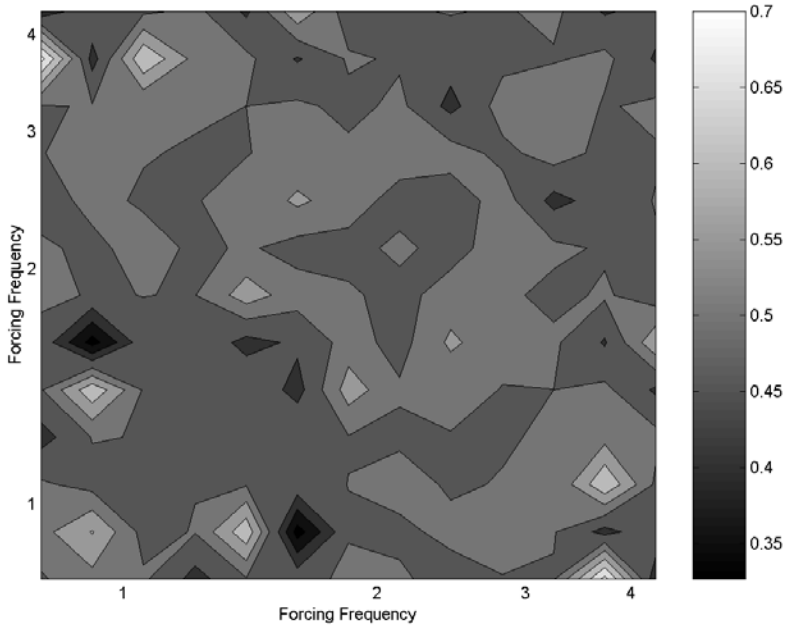

Figure 5.10: Optimum SSA location in the x direction on the plate as function of two forcing frequencies

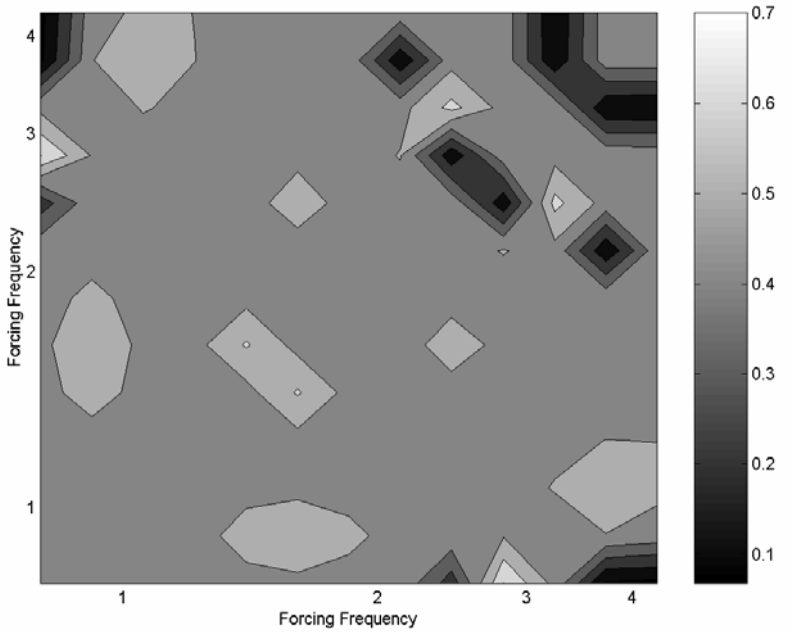

Figure 5.11: Optimum SSA location in the y direction on the plate as function of two forcing frequencies

frequency of the first plate mode. As can be seen from these figures, the attachment point was to found to be near 0.5 in both directions for nearly the entire range of forcing frequencies. This corresponds to an attachment point near the geometric center of the plate. The first mode shape of the plate has the largest amplitude of vibration at the center of the plate. Therefore, the absorber is controlling this mode of vibration when attached at the midpoint of the plate. To achieve optimal control of the plate, the SSA is attached near the center of the plate to control the fundamental vibration mode for nearly all of the forcing cases considered.

Figures 5.12 and 5.13 together define the optimal state-switched absorber tuning frequencies for a range forcing frequency combinations. Figure 5.12 plots the mean of

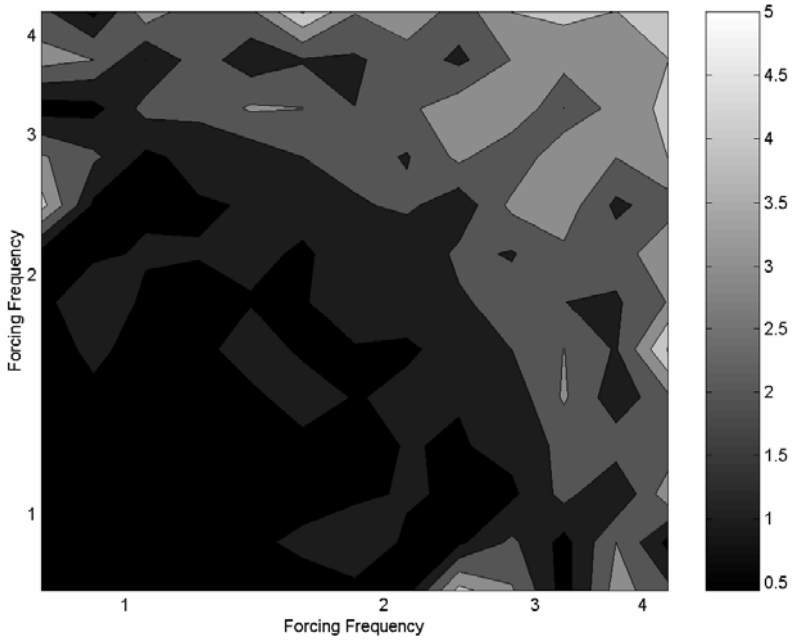

Figure 5.12: Mean of two SSA tuning frequencies normalized by first mode of plate as function of two forcing frequencies

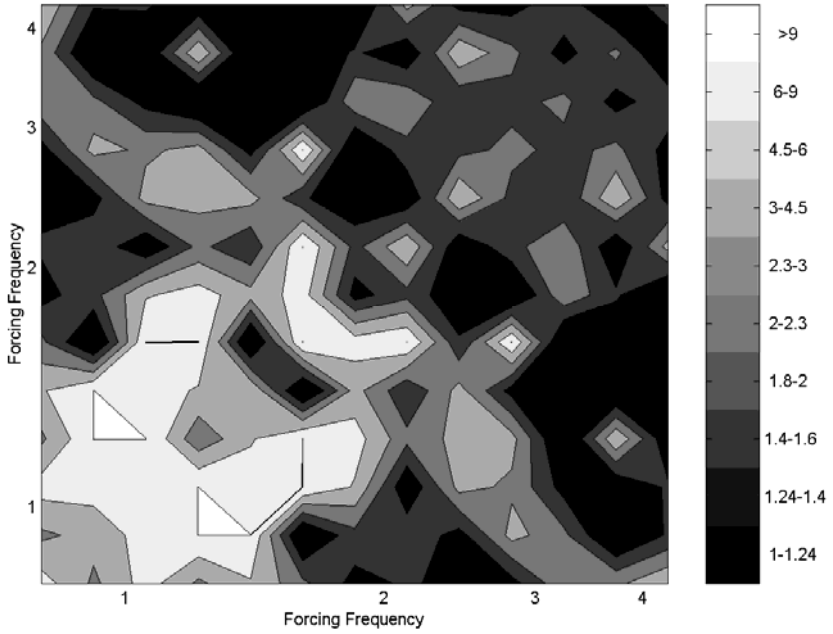

Figure 5.13: Ratio of optimum SSA tuning frequencies for a plate as function of two forcing frequencies

the two optimized SSA tuning frequencies as a function of the two forcing frequencies. All frequencies are normalized by the natural frequency of the fundamental mode of the isolated plate. As was the case for the beam optimization, the average SSA tuning frequency increases with increasing forcing frequency. Figure 5.13 plots the ratio of the upper SSA frequency to the lower SSA frequency as a function of the two-excitation frequencies. Note, there are very few forcing cases that resulted in an SSA frequency ratio at or very near one. With such a tuning, the SSA would represent a classical tuned vibration absorber as switching between discrete frequencies would not occur. As stated previously, for some forcing cases considered, the global optimum is a TVA. However, the simulated annealing algorithm often did not find this global optimum, when it existed, for the SSA applied to a plate. The plate system adds a new location parameter to that of

the beam system, therefore increases the complexity of the system and offers more opportunities for local minimums. While the simulated annealing algorithm always finds a low plate kinetic energy, it is not guaranteed to find the lowest plate kinetic energy. Also, Figure 5.13 seems to show the opposite of what was found for the tuning frequency ratio of the beam system. At forcing frequencies less than two, where good performance of the SSA occurred, the tuning frequency ratio is above 6 for most of that frequency range. Good performance of the SSA applied to a plate can require large spacing between the tuning frequencies, whereas good performance of the SSA applied to a beam generally requires tuning frequency ratios less than 2. However, the tuning frequency ratio corresponding to the best relative performance of the SSA applied to a plate was only 1.24. As with the beam system, there is no correlation between the forcing frequencies and the optimal tuning frequencies. Therefore, there is no way to determine the optimal tuning frequencies given a set of forcing frequencies.

CHAPTER 6

EXPERIMENTAL SETUP

This chapter outlines the setup of the beam and plate experiments used to validate the performance of the state-switched absorber used for vibration control. A direct search to find the best performing absorber for each of a number of forcing cases was done from a set of potential tuning frequencies attainable by a fabricated SSA. The same parameters were used using the simulations described in Chapters 4 and 5 to predict the performance of the SSA. The results from the experiments were compared to the results from the simulations to experimentally validate the simulations. The first section in this chapter details the magneto-rheological elastomer implementation of the state-switched absorber. The beam and plate systems to which the SSA is attached are then described. Next, the instrumentation, including the sensors, actuators, and DSP system, used in the experiments are detailed. The final section in this chapter lays out the procedures used to acquire the data.

STATE-SWITCHED ABSORBER DESIGN

Magneto-rheological elastomers (MRE) were used to fabricate an absorber that can switch between discrete stiffnesses. An MR elastomer is a rubber that has fine iron particles dispersed throughout. A magnetic field is applied during the cure of the elastomer to align the iron particles in chains. The stiffness of the cured MRE is dependent on the magnetic field applied across the elastomer; the higher the magnetic flux, the greater the stiffness. This stiffness' dependence on the magnetic flux was

utilized in designing an SSA with variable discrete stiffnesses. For more detail on the properties of MR elastomers, please refer to the paper by Albanese and Cunefare.[46]

Figure 6.1 illustrates the magneto-rheological elastomer implementation of the state-switched absorber. This absorber design was employed for the experiments to validate the SSA's performance in reducing vibrations in continuous systems. The design consists of four MREs and an electromagnetic coil, along with steel to close the magnetic circuit. The electromagnetic coil is simply a spool of magnet wire wrapped around an iron core. By running an electric current through the coiled wire, a magnetic flux is created through the core of the coil. As seen in Figure 6.1, this flux continues into the vertical steel members and then through the MR elastomers. Since the MREs contain iron particles aligned in chains, the flux moves through the elastomer, thus causing an increase in stiffness as compared to when no flux exists. The magnetic circuit is completed by thin steel strips along the top and bottom of the absorber. These strips are

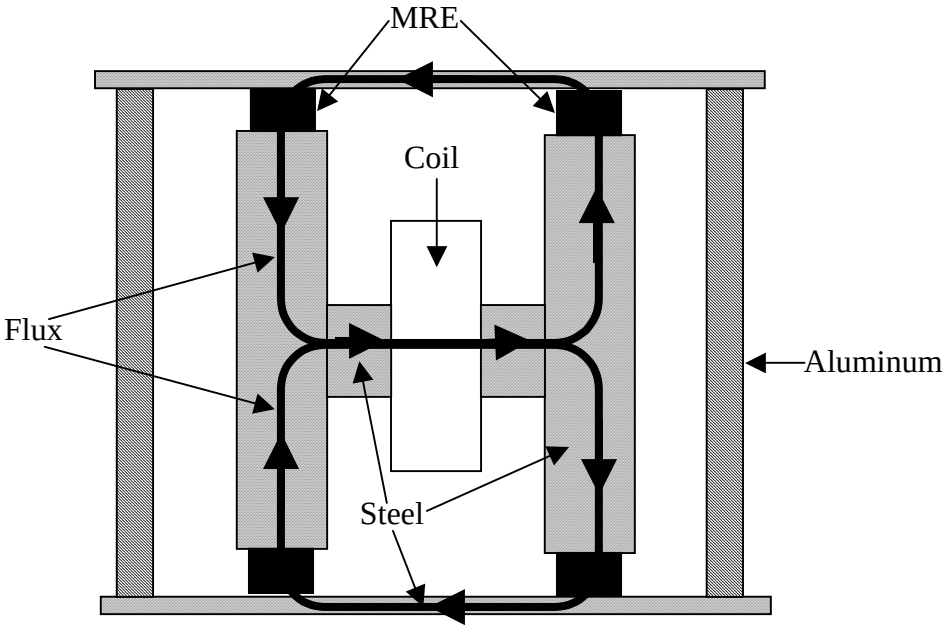

Figure 6.1: MR elastomer implementation of a state-switched absorber.

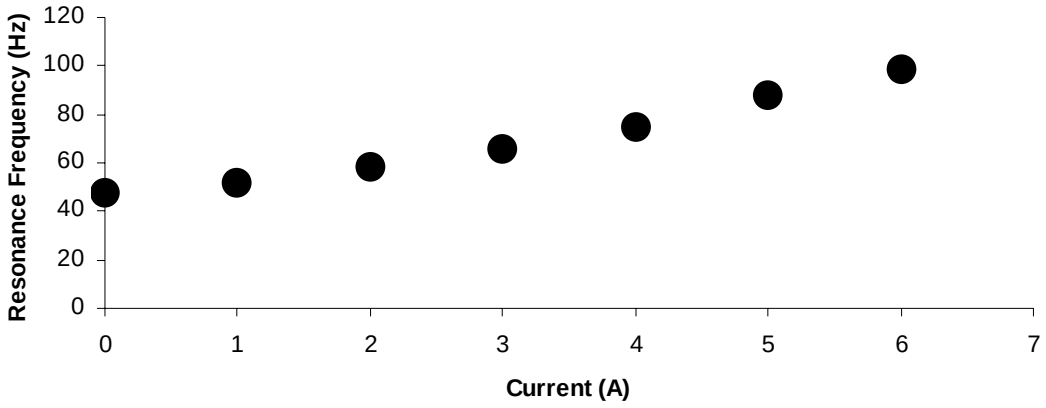

Figure 6.2: SSA resonance frequencies as a function of electromagnet current

separated by aluminum rods and are rigidly attached to the base to which the absorber is attached. Aluminum is used as the supports so the magnetic flux path would consistently pass through the MR elastomers. The electromagnet and the larger steel members become the absorber mass (132 grams), while the MR elastomers are the stiffness and damping elements of the absorber.

Figure 6.2 plots the resonance frequencies of the state-switched absorber described above as a function of the electrical current supplied to the electromagnet. As can be seen, there is an increase in resonance frequency with an increase in electrical current. The frequency with no current applied is 48 Hz, whereas at 6 amps, the resonance frequency is 98.9 Hz. Therefore, the SSA has a capability to change its frequency by 106% and it stiffness by 325%.

BEAM AND PLATE SETUP

To experimentally validate the vibration control performance of the state-switched absorber applied to continuous systems, comparison of an experimental and numerical SSA performance for a fixed set of tuning parameters was done for both a beam system and a plate system. The experimental setup of each system is described in the following sections. The first section details the cantilever beam setup. The beam setup is followed by a description of the plate system used in the experiments.

Beam Setup

A cantilever beam was used to validate the performance of an SSA applied to a beam. To examine the effect of the state-switched absorber at multiple beam modes, two beams were used for experimentation. This is due to the fact that the frequencies of the first and second cantilever beam modes are further apart than range of tuning frequencies available in the absorber described above. Therefore, one beam is designed such that the frequency of the first mode is near 60 Hz, which was chosen such that the potential SSA tuning frequencies lie both above and below the mode of interest, and another beam is designed so the second mode is about 60 Hz. Also, each beam should be wide enough to attach the absorber to it, about 4 inches, and have a mass roughly 10 times the mass of the absorber, about 1.32 kg.

The first beam was made from aluminum and was 4 inches wide, 0.5 inches thick, and 17 inches long. This resulted in a beam that had a mass of 1.5 kg. Given the absorber had a mass of 132 g, the absorber to base mass ratio for the first beam is 0.09. The second beam was made from steel and was 4 inches wide, 0.125 inches thick, and

19.5 inches long resulting in a mass of 1.3 kg and an absorber to base mass ratio of 0.1. Figures 6.3 and 6.4 plot the frequency response of each beam. As can be seen from Figure 6.3, the first vibration mode of the aluminum beam occurs at 58.6 Hz, near the predicted natural frequency of 60 Hz and within the SSA tuning frequency range of 48 Hz to 98.9 Hz. Figure 6.4 illustrates that the frequency of the second mode of the steel beam is 64 Hz, also close to the predicted value and within the SSA frequency range. The SSA will attempt to control the first mode of vibration in the aluminum beam and the second vibration mode in the steel beam. The unlabeled peaks in the frequency responses shown Figures 6.3 and 6.4 are resonances due to torsional modes within the beam. In the experimental beam, there are torsional degrees of freedom that are not captured in the beam model. This torsional freedom will therefore lead to observable frequencies in the

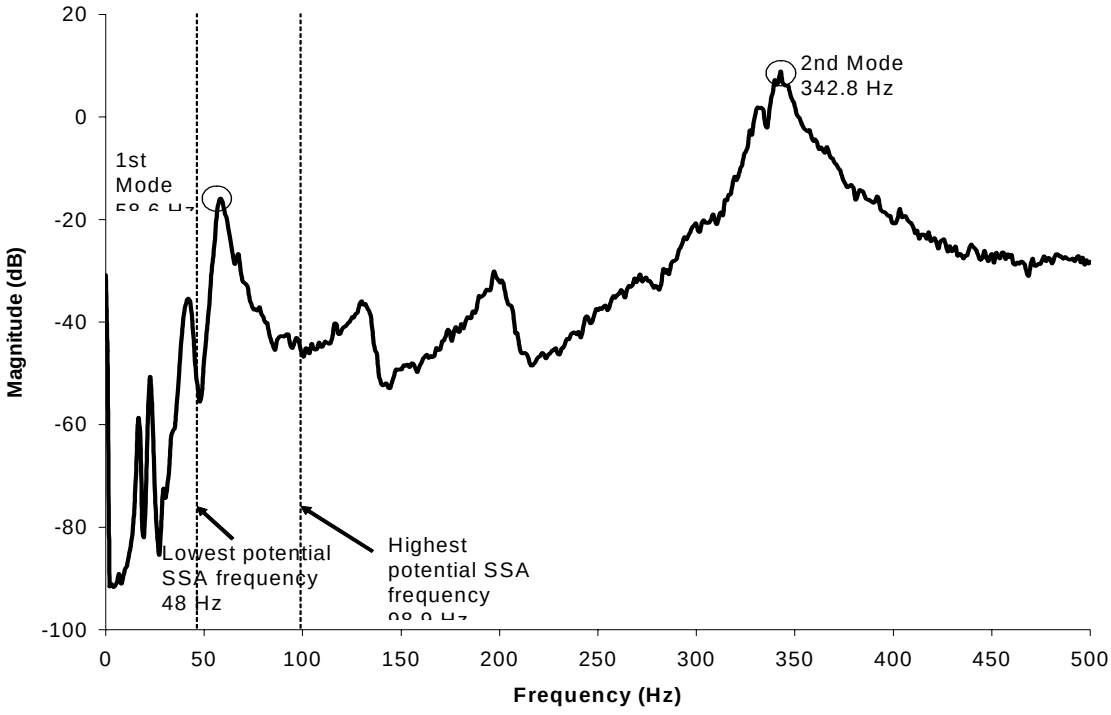

Figure 6.3: Frequency response of cantilever aluminum beam

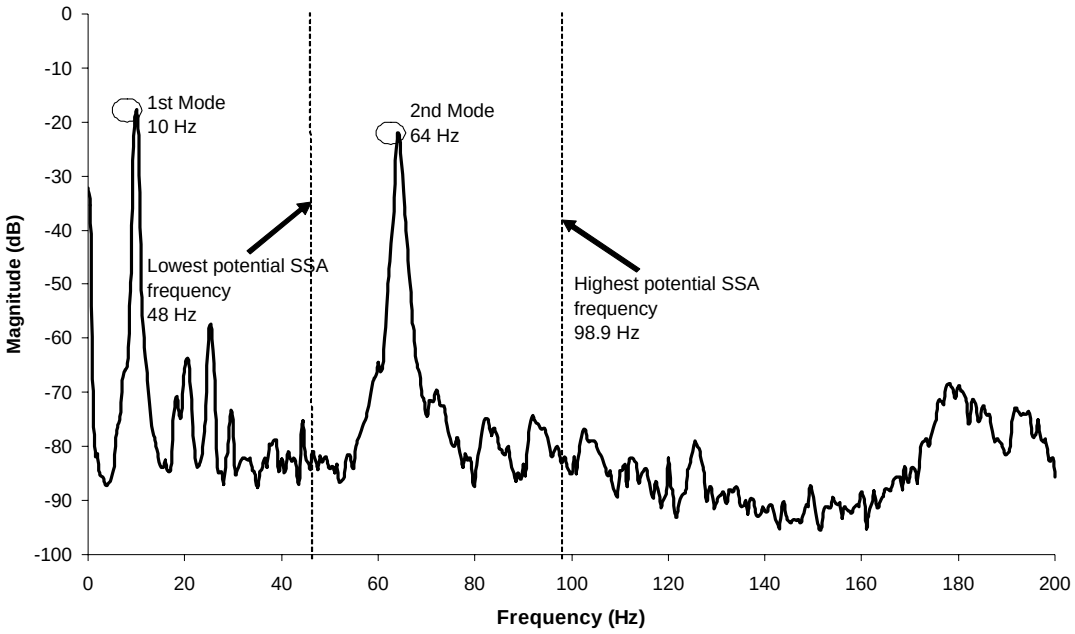

Figure 6.4: Frequency response of cantilever steel beam

response that are not predicted by the simple beam model.

Plate Setup

Only one plate was used to validate the SSA's performance, as the natural frequencies of the plate modes are closer together than those of the beam modes, therefore more than one plate mode is within the switching limits of the physical state-switched absorber. The coil on the SSA used for the beam experiments burned out, so a new absorber was built for the plate experiments. Figure 6.5 plots the resonance frequency of the new absorber versus the input current. As can be seen from Figure 6.5, the lowest possible frequency of the new SSA is 56.9 Hz while the highest possible frequency is 102.1 Hz. This results in a potential frequency shift of 79.4%.

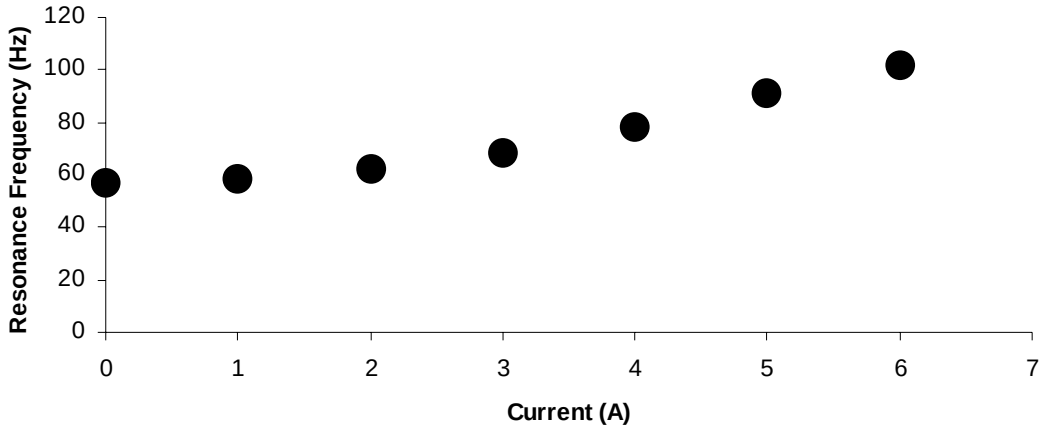

Figure 6.5: SSA frequencies versus current for plate experiments

A plate was designed so that several vibration modes would be within the range of frequencies between which the SSA is capable of switching. A square plate clamped on all four sides was used for the experiments, similar to that used in the numerical optimization. The plate used in the experiments was fabricated using a 0.0312 inch steel sheet clamped so that each side was 18.25 inches in length. These dimensions resulted in a plate that had a mass of 1.35 kg and an absorber to base mass ratio of 0.1. The frequency response of the plate is shown in Figure 6.6. The region between dashed lines in Figure 6.6 is the range of potential frequencies of the state-switched absorber. As can be seen, the potential switching frequency range covers a number of natural frequencies of the plate. The SSA will attempt to control these vibration modes of the plate.

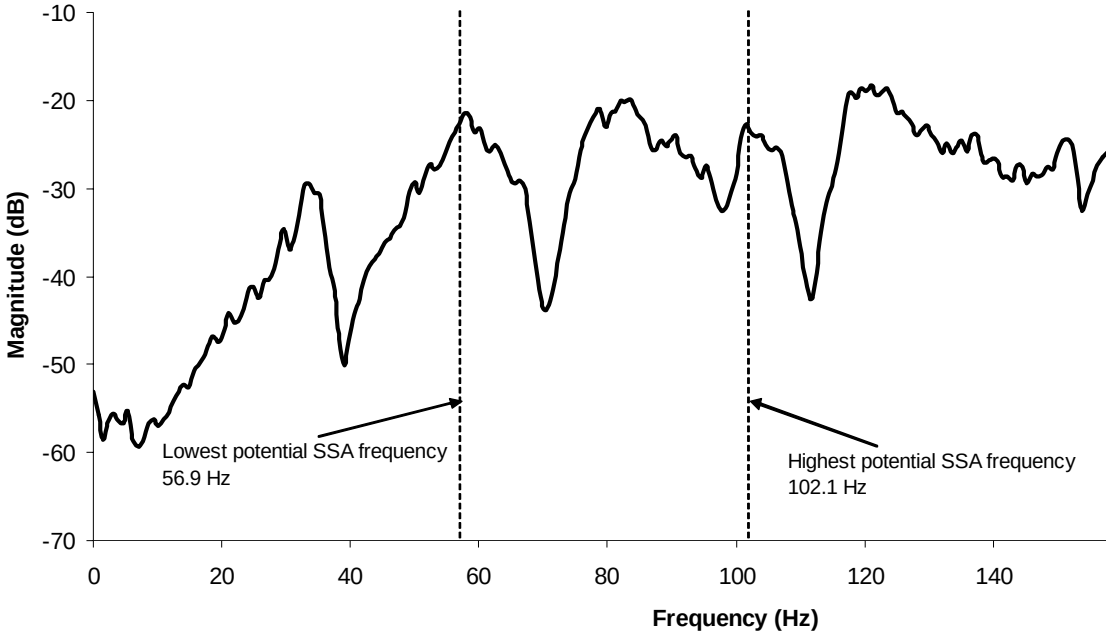

Figure 6.6: Frequency response of plate

INSTRUMENTATION

Figure 6.7 depicts the experimental setup of the beam system, including all the sensors and actuators. Three accelerometers and an impedance head, which measures both force and acceleration, are distributed along the length of the beam and are used to measure the response. Kistler 8636C50 accelerometers and a Kistler 8770A50 impedance head were used. The impedance head also measures the force delivered to the beam using an LDS V203 shaker. The connection point for the excitation is the center of the cantilever beam, as was used in the numerical optimization. The state-switched absorber's base is rigidly attached to the beam and a Philtec D100-QPT displacement probe is rigidly attached to the base of the SSA. This displacement probe measures the relative displacement between the SSA and the beam at the absorber attachment point.

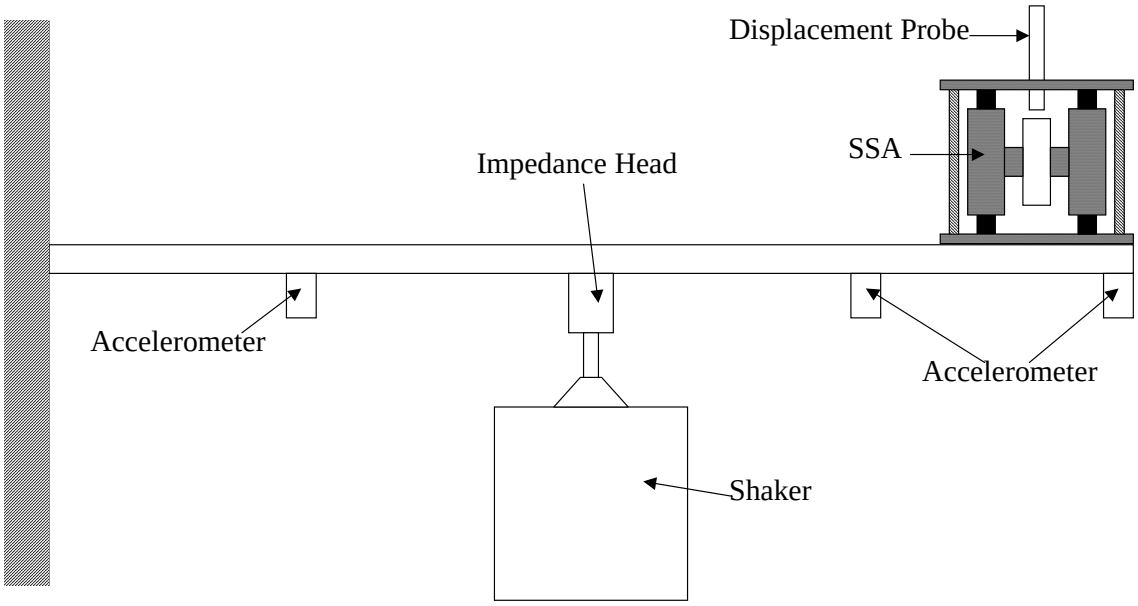

Figure 6.7: Experimental setup with sensors and actuators

The system is controlled using a dSpace DS1103 digital system processing system. To implement the switching control algorithm defined by Equations (2.2) and (2.3) the displacement probe and the accelerometer with the same beam attachment point as the SSA are used. The displacement probe determines when the absorber has passed through a zero strain condition. By differentiating the displacement signal, the relative velocity is calculated which is needed in Equation (2.3). To find the base velocity needed to determine when to switch, the signal from the accelerometer with the same attachment point as the SSA is integrated. To perform a switch, an electrical current is sent to the electromagnetic coil using a Kepco 36-6D bipolar operational power supply.

The plate system has a similar setup with respect to the sensors and actuators, except the plate system contains more accelerometers to more accurately capture the response of the system. Figure 6.8 depicts the locations of all the accelerometers, the impedance head, and the various attachment locations of the absorbers. The points

labeled SSA_i represent potential attachment points of the state-switched absorber. Only one absorber is attached to the plate at any given time. These attachment points were chosen based on the results of the numerical optimization detailed in Chapter 5 and represent a set of three potential attachment points for the numerical and experimental direct search used to experimentally validate the SSA simulations. Each a_i in Figure 6.8 represents a location of an accelerometer. These were placed based on either corresponding to an SSA location or to avoid a nodal point on the plate for the modes of interest. F and a_4 correspond to the impedance head, which measures the acceleration and force at the point of excitation. The excitation point was also chosen to avoid a node on the plate.

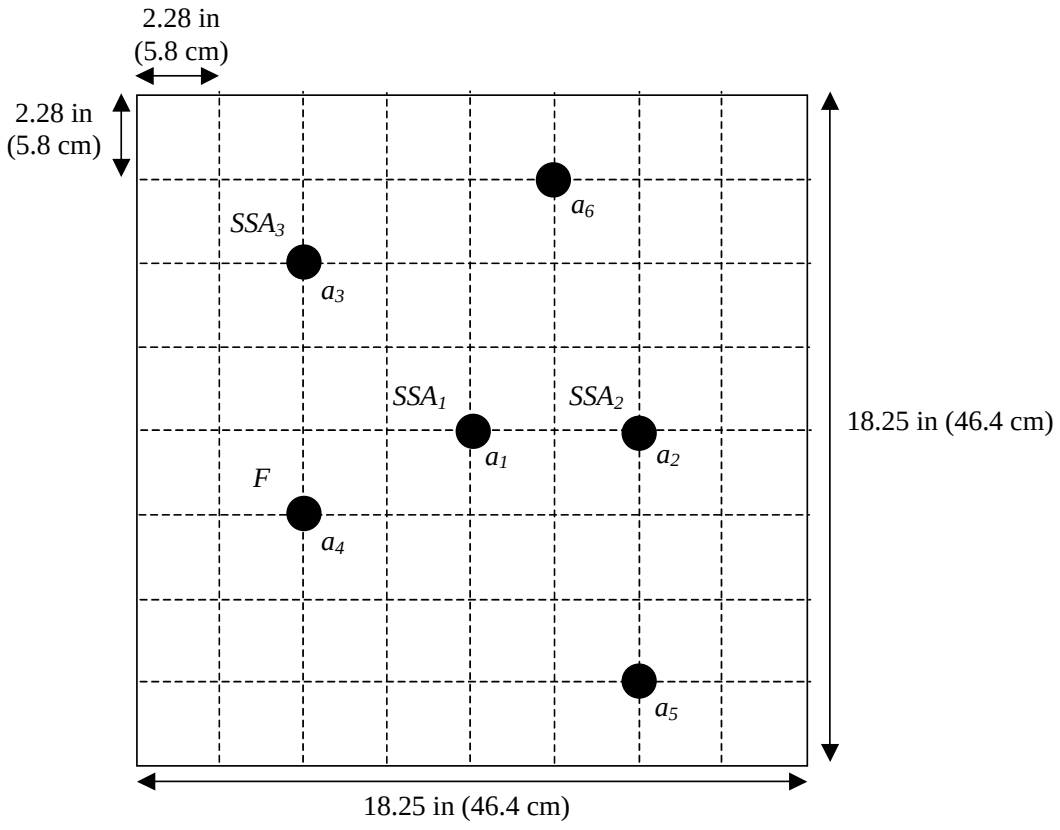

Figure 6.8: Plate layout including accelerometers, force transducer, and SSA locations.

PROCEDURES

The purpose of the experimental work at hand is to show how the state-switched absorber performs compared to a tuned vibration absorber when attached to both a beam and plate. The experiments were also performed to determine how closely the simulations predict the performance of the SSA. The procedures described here were developed to compare the performance found experimentally to the performance predicted by the numerical simulations. The specifics of the procedures used for both the beam and plate are outlined in the following sections.

Beam Procedures

Each of the two beams considered in the experiments was subjected to a range of two-frequency component excitations similar to that in the simulations done previously. Table 6.1 shows the excitation frequencies stepped through for each beam. There are seven discrete forcing frequencies stepped through for the aluminum beam resulting in 28 forcing combinations, including single frequency component excitations. The steel beam has five discrete excitation frequencies resulting in 15 combinations. These sets of excitation and tuning frequencies were also used in numerical simulations to predict the performance of a SSA as compared to a TVA.

Table 6.1: SSA tuning frequencies and forcing frequencies for both beam experiments

SSA Frequencies	
Current (A)	Frequency (Hz)
0	48.0
1	51.4
2	58.7
3	65.4
4	74.9
5	88.1
6	98.9

Forcing Frequencies (Hz)	
Aluminum Beam	Steel Beam
50.0	50.0
54.0	56.0
58.0	64.0
66.0	77.0
74.0	95.0
84.0	
95.0	

A direct search of the set of tuning frequencies shown in Table 6.1 was done experimentally to find the best performing TVA and SSA for each two-frequency forcing combination. Also, simulations were performed for each forcing and tuning case considered in the experiments to determine how well the simulations predict SSA performance. Instead of attempting to reproduce the optimization, this procedure was used because of the high sensitivity of the optimization results and the capabilities of the fabricated SSA. An SSA fabricated using MREs cannot produce the tuning frequencies with a tolerance on frequency performance within the limits implied by the sensitivity results detailed in Chapter 5. Also, the fabricated SSA cannot produce a large enough frequency shift to reproduce many of the results found in the optimization.

For experimental comparison between an SSA and a TVA, the best performing TVA and SSA must be found for each forcing case. The attachment location and both tuning frequencies that result in the best performance of each absorber should be found. The optimization study showed that the location of the absorber should be located at the free end of the beam when the excitation frequencies are near the first mode and in the middle of the beam when controlling the second mode of vibration. Therefore, the absorber was attached at the free end of the aluminum beam and the center of the steel

beam. To find the tuning frequencies that resulted in the best absorber performance, a direct search was employed by stepping through a range of SSA resonance frequencies. Table 6.1 contains the potential SSA frequencies and the corresponding electrical current needed to achieve each frequency. There are seven discrete frequencies which make up the whole set of potential absorber tuning frequencies. Combining these potential states in groups of two tuning frequencies, including equivalent frequencies where the absorber acts as a TVA, result in 28 different absorber tuning frequency combinations. For each forcing case considered, each of the 28 absorber tuning combinations were stepped through to determine which tuning parameters resulted in the best performance. To determine how well the model predicts the actual system, the SSA performance was also found using the simulations described earlier for each of these same forcing and tuning cases considered in the experiments.

For each forcing frequency combination investigated experimentally, the shaker is enabled and allowed to excite the beam. While the voltage amplitude sent to shaker is held constant, each tuning combination is stepped through, acquiring five seconds of the beam's response for each frequency combination. This acquisition time was found to be adequate by running some trials and observing the time to pseudo-steady state and period of repetition in the response. Pseudo-steady state occurred in less than one second and the longest period repetition found during all testing was on the order of 0.5 seconds. The kinetic energy of the beam is calculated for each tuning combination by

$$\frac{2T}{M} = v^T v = \begin{bmatrix} v_{accel1} & v_{accel2} & v_{accel3} & v_{accel3} \end{bmatrix} \begin{bmatrix} v_{accel1} \\ v_{accel2} \\ v_{accel3} \\ v_{accel4} \end{bmatrix} \tag{6.1}$$

where M is the mass matrix of the beam and v_{accel} is the velocity at each accelerometer attachment point, calculated by integrating each accelerometer's signal. The root-mean-squared value of the kinetic energy is calculated for the final 2.5 seconds of the response and normalized by the rms force, measured from the impedance head. Even though the kinetic energy is not averaged over a repetition interval, the maximum possible error averaging over the final 2.5 seconds given a maximum repetition interval of 0.5 seconds is a negligible 0.012 dB. This final energy metric can be written as

$$KE_{metric} = \frac{T_{rms}}{F_{rms}}. \tag{6.2}$$

The kinetic energy is normalized by the force for accurate comparison between tests. The lowest kinetic energy metric is found from all the tunings where the resonance frequencies are equal, thus finding the best performing TVA. The same is done for the tuning cases with unequal frequencies to determine the best performing SSA. Comparison of the best performing SSA and TVA is done for each forcing case in the experiments.

For each forcing and tuning combination, simulations were also done to find the SSA performance. These simulations were performed similarly to those described in Chapters 4 and 5. The SSA performance found through simulations was force normalized similarly to that of the experiments, which is described in Equation (6.2). The predicted SSA performance was then compared to the performance found

experimentally for each forcing and tuning case considered in the experiments. This comparison is done by calculating the ratio of the experimental performance of the SSA to the performance found through the simulations for each forcing and tuning combination. As a metric of how well the simulations predicted the observed performance, the standard deviation of all these ratios for both beams is then calculated.

Plate Procedures

The procedures used to examine the plate system are very similar to those used in testing the beams. As in the beam experiments, the plate was subjected to several two-frequency component excitations. For each forcing case, several tuning combinations were used to determine the optimal tuning for each of the state-switched absorber and the tuned vibration absorber. The potential forcing and tuning frequencies used in the plate experiments our shown in Table 6.2. Six discrete forcing frequencies were used in the plate experiments, resulting in 21 different forcing combinations. For each forcing case, seven different tuning frequencies were stepped through to determine the best performing absorbers, resulting in 28 different tuning combinations. Also, the absorber was placed at each of three attachment locations for each forcing case. These attachment points can be

Table 6.2: SSA tuning frequencies and forcing frequencies for the plate experiments

SSA Frequencies	
Current (A)	Frequency (Hz)
0	56.9
1	58.4
2	62.1
3	68.1
4	77.9
5	91.3
6	102.1

Forcing Frequencies (Hz)
56.0
63.0
72.0
81.0
91.0
103.0

seen in Figure 6.8. The kinetic energy of the plate was calculated using Equations (6.1) and (6.2) outlined above. For each forcing case, the location and tuning that resulted in the lowest force normalized kinetic energy for both the SSA and the TVA were determined experimentally. These best performing absorbers were then compared to determine whether the SSA performed better than the TVA for each excitation case. Also, the SSA performance predicted through the simulation of each forcing, tuning, and location combination was compared to the performance observed in the experiments.

CHAPTER 7

EXPERIMENTAL VALIDATION RESULTS

The following sections present the results from the experimental validation of the beam and plate systems. The results of the direct search found experimentally and presented here. Also, the observed SSA performance is compared to the performance predicted through numerical simulations. The first section details the results from the beam experiments, while the last section discusses the results from the plate experiments.

BEAM RESULTS

Experiments were performed attaching a state-switched absorber to two cantilever beams. The purpose of the experiments was to compare the performance achieved using an SSA to the performance achieved using a TVA. The experiments were also done to determine the how well the simulations predicted the performance of the SSA. One beam's first vibration mode was within the range of tuning frequencies of the state-switched absorber while the other beam was designed such that its second mode was within the SSA's tuning limits. A direct search of a fixed set of tuning parameters was used to experimentally find the best performing SSA and TVA for each of a number of two-frequency excitations. The best performances of each absorber were compared to determine if the SSA showed improved performance versus a classical TVA. Also, the SSA performance found experimentally was compared to the performance calculated from numerical simulations using the same tuning parameters. Specifics of the setup and procedures for these experiments were outlined in the previous chapter.

Before comparing the performance of the SSA to that of a TVA and comparing the experimental results to the simulations, the experimental beam response with an SSA attached is compared to the experimental response of an untreated beam. Figures 7.1 and 7.2 show the ratio of the kinetic energy of the beam with the best performing SSA attached to that untreated beam's kinetic energy as a function of the two forcing frequencies. The forcing frequencies are normalized by the natural frequency of the fundamental mode of vibration of each beam. The force-normalized kinetic energy is found using Equations (6.1) and (6.2) for each forcing case. The ratio is plotted in Figures 7.1 and 7.2 using a dB scale defined as

$$KE_{ratio} = 10\log\left(\frac{KE_{SSA}}{KE_{untreated}}\right). \tag{7.1}$$

When the value found in Equation (7.1) is negative, the beam treated with the SSA has

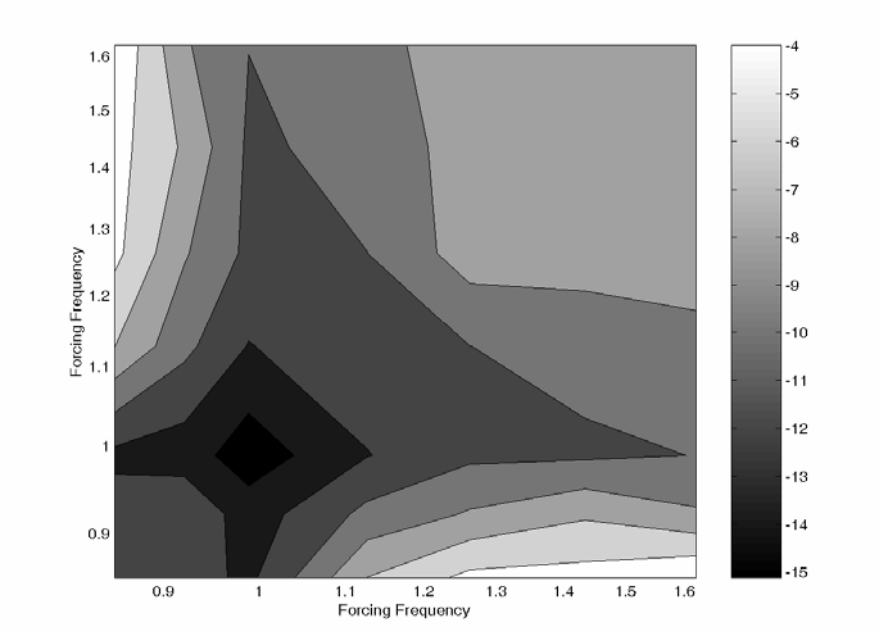

Figure 7.1: Experimental kinetic energy ratio, in dB, of the aluminum beam with SSA attached to untreated beam. Forcing frequencies near first mode of vibration.

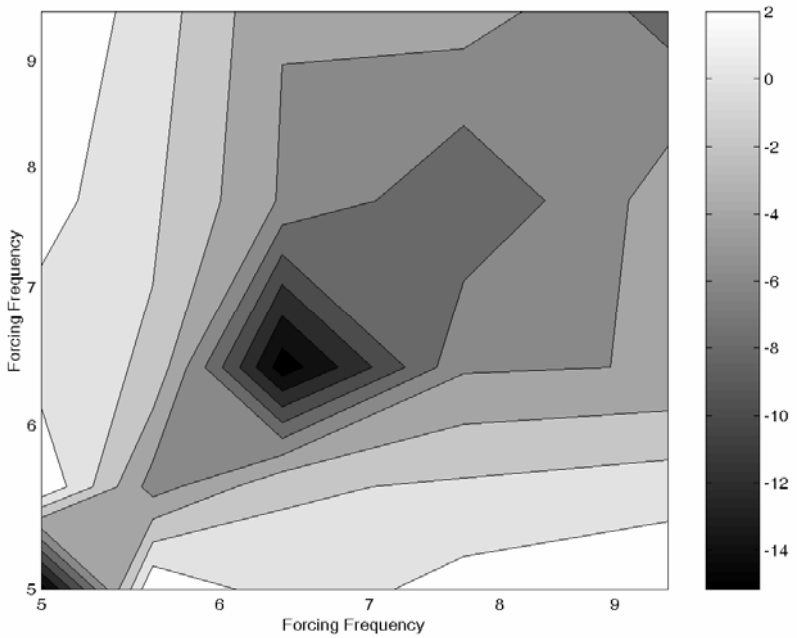

Figure 7.2: Experimental kinetic energy ratio, in dB, of the steel beam with SSA attached to untreated beam. Forcing frequencies near second mode of vibration.

improved performance versus the untreated beam. As can be seen from Figures 7.1 and 7.2, attaching an SSA reduces the vibration of a beam for nearly the entire range of forcing frequencies considered for both beams. The best performance of the aluminum beam, whose first mode is at 58.6 Hz, occurs when the normalized forcing frequencies are both one, corresponding to the frequency of the first mode of vibration, with an improved performance of 15.1 dB. The best performance of the steel beam, whose second mode occurs at 64 Hz, occurs when the normalized forcing frequencies are both 6.4, corresponding to an excitation near the frequency of the beam's second mode. The SSA reduces the vibration by 15.2 dB for this forcing case. There is a small region where the SSA does not reduce the vibration of the steel beam. The worst SSA performance on the steel beam resulted in a 2 dB increase of the beam kinetic energy. However, this

increase is very small when compared to the largest decrease in kinetic energy of 15.2 dB.

The results of the experiments comparing the performance of the state-switched absorber to the tuned vibration absorber performance are depicted in Figures 7.3 and 7.4. In these figures, the ratio of the kinetic energy of the best performing SSA beam to the best performing TVA beam's kinetic energy is plotted versus the two forcing frequencies, normalized by the beam's fundamental frequency. The ratios in these figures are shown in dB, calculated similarly to the untreated beam ratio defined by Equation (7.1). As shown in Figures 7.3 and 7.4, for the entire range of forcing frequencies considered, the ratio is less than 0 dB. Therefore, an optimized SSA reduces the beam vibration more than an optimized TVA for each forcing case considered. The best relative performance

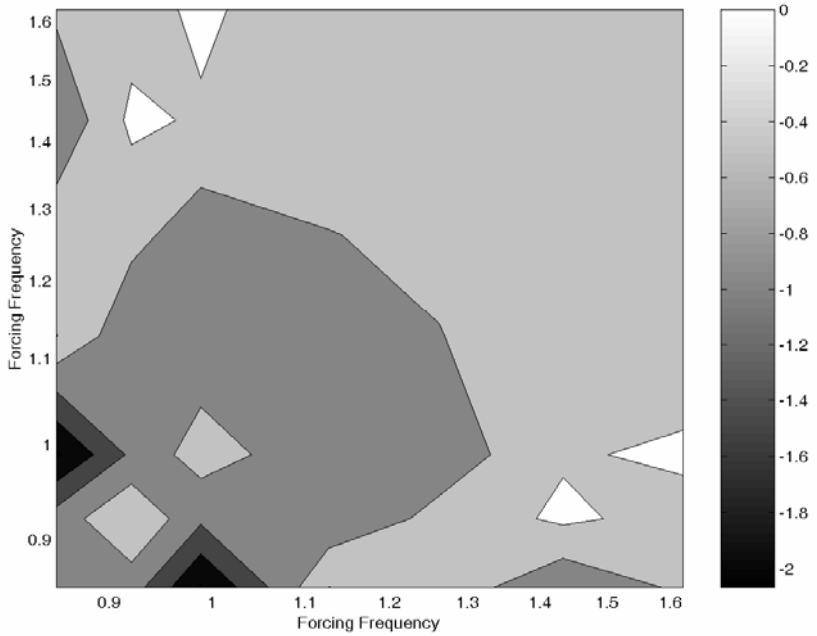

Figure 7.3: Experimental kinetic energy ratio, in dB, of beam with SSA attached to beam with TVA attached. Forcing frequencies near first mode of vibration.

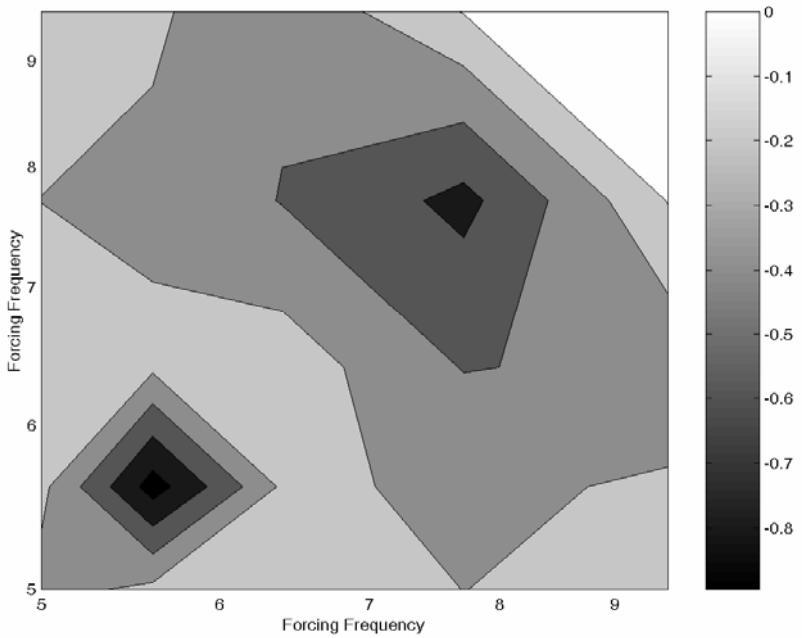

Figure 7.4: Experimental kinetic energy ratio, in dB, of beam with SSA attached to beam with TVA attached. Forcing frequencies near second mode of vibration.

of the SSA attached to the aluminum beam, where the SSA is controlling the first mode, occurs when the normalized forcing frequencies are 0.85 and 0.99 with a 2.1 dB reduction in vibration versus the TVA. For the steel beam, the greatest improvement versus the TVA is 0.9 dB and occurs when both normalized frequencies are 5.6. For the entire range of excitations for both beams, the state-switched absorber performs better than a classical tuned vibration absorber at controlling beam vibrations.

A repeatability study of the SSA was also performed for one forcing and tuning combination, specifically when the normalized forcing frequencies 0.92 and 1.13 and the normalized SSA tuning frequencies are 0.82 and 1.00. The experiment was performed ten times for this specific case and the normalized beam kinetic energy was found for each trial. The mean and the standard deviation from the mean of the kinetic energies

were calculated for each of the ten trials. To quantify the repeatability of the experimental SSA, the standard deviation was divided by the mean. This ratio was found to be 0.126, which corresponds to 0.52 dB. This ratio means that the standard deviation of these ten trials was 12.6% of the average kinetic energy. This results follows the repeatability results found for MREs by Albanese and Cunefare.[46]

To determine how well numerical simulations predict the performance of the SSA, each forcing and tuning considered in the experiments was put into the numerical simulations described earlier. For each test case, the force normalized beam kinetic energy was calculated from the simulation and divided by the experimental kinetic energy giving a performance ratio of the simulations to the experiments. The simulations predicted the observed performance relatively well. The standard deviation from an energy ratio of 1, the ratio at which the simulation perfectly predicted the experiment, for all the tuning and forcing combinations of both beams was 0.101, which corresponds to 0.41 dB. Note, that the standard deviation from experiment to experiment is 0.52 dB as compared to a 0.41 dB standard deviation between experiment and simulation. This means that the error in the prediction is within the error limits of the experiments. Therefore, the simulation predicts the observed SSA performance from the experiments quite well.

PLATE RESULTS

Experiments and simulations using an SSA were also performed on a vibrating clamped plate. The plate was subjected to a number of two-frequency component excitations. For each forcing case, the tuning frequencies and attachment location for the best performing SSA and a TVA were found using a direct search method for the

experiments. These experiments were executed to determine the performance of an SSA compared to that of a classical tuned vibration absorber as well as to validate the results found through the numerical simulations. For more details on the setup and procedures of the plate experiments, please refer to Chapter 6.

Figure 7.5 depicts the experimental ratio of the kinetic energy found of the plate with a state-switched absorber attached to the kinetic energy of an untreated plate as a function of excitation frequencies normalized by the frequency of the fundamental plate mode. This ratio is plotted using a dB scale defined in Equation (7.1) above. When this ratio is less than 0 dB, the SSA reduces the kinetic energy of the vibrating plate. As can be seen from Figure 7.5, the SSA reduces the vibration of the plate for the entire range of forcing frequencies considered. The state-switched absorber achieves its greatest

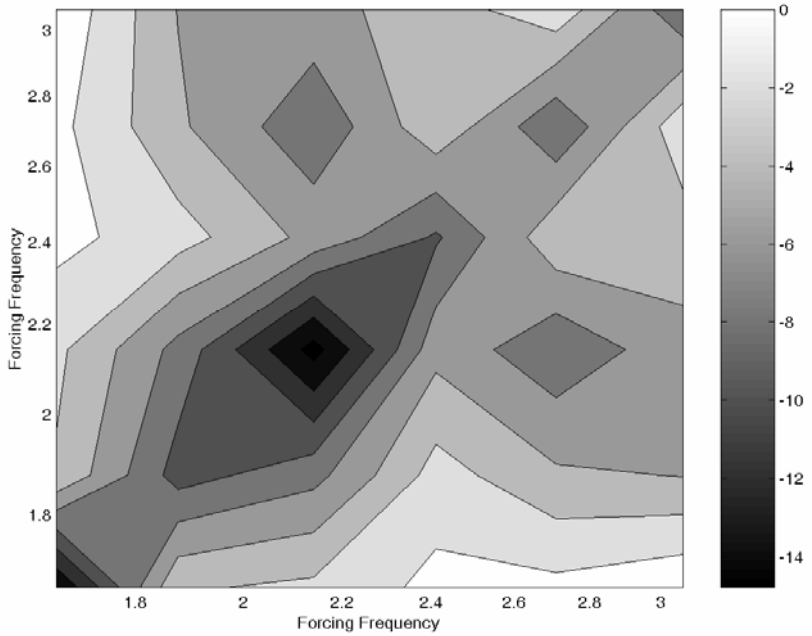

Figure 7.5: Experimental kinetic energy ratio, in dB, of the plate with SSA attached to untreated plate.

vibration reduction of 14.8 dB when both normalized forcing frequencies are 2.14, which is in the vicinity of the plate's natural frequency near the middle of the potential SSA frequency range.

Figure 7.6 depicts the observed ratio of the plate kinetic energy with the state-switched absorber attached to the plate kinetic energy with the tuned vibration absorber attached. Again, when this ratio is less than 0 dB the SSA reduces plate vibration more than a TVA in the experiments. Over the entire range of forcing frequencies considered, the ratio is less than 0 dB meaning that the SSA outperforms the TVA for each forcing case. The best relative performance of the SSA as compared to the TVA occurs when the normalized excitation frequencies are both 1.88, where the SSA outperforms the TVA by 2 dB.

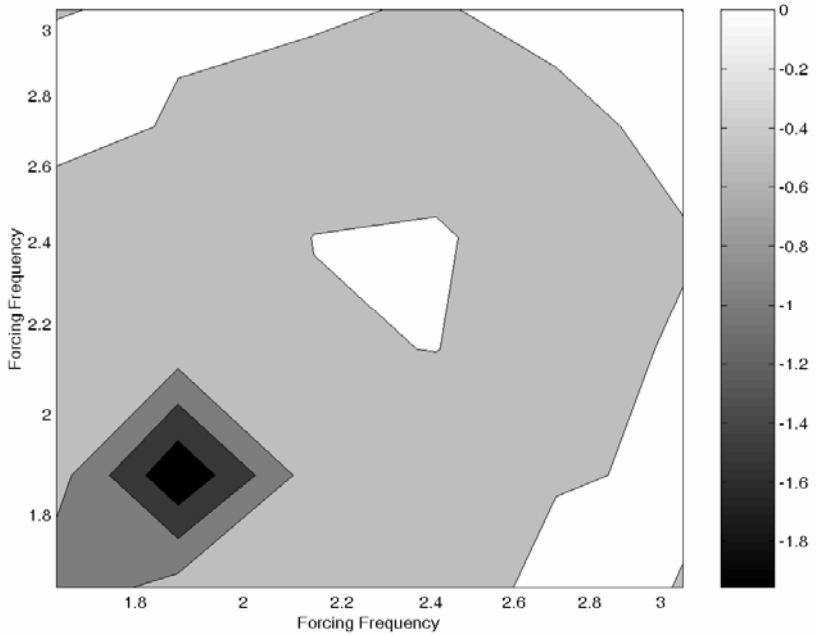

Figure 7.6: Experimental kinetic energy ratio, in dB, of a plate with SSA attached to a plate with TVA attached.

To determine the repeatability of the plate experiments a single forcing and tuning case was selected and the experiment was repeated ten times, just as in the beam experiments. The specific case here was when the normalized forcing frequencies were 1.88 and 2.14, the normalized SSA tuning frequencies were 1.69 and 2.03, and the SSA attachment point was in the center of the plate. The standard deviation of the normalized kinetic energies divided by the mean of the kinetic energies for all plate experiments was calculated to be 0.144, which corresponds to 0.59 dB. This indicates that the standard deviation in the plate kinetic energy found from these experiments is 14.4% of the mean kinetic energy. This repeatability result is very similar to those found in the beam experiments.

To determine how well the simulations predicted the SSA performance, simulations were performed for each of tuning and forcing cases considered in the plate experiments. Similarly to the beam system, the ratio of the plate kinetic energy found from the simulation to the kinetic energy found from the experiments was found for each forcing and tuning combination. When this ratio equals 1, the simulation exactly predicts the experiment. Therefore, the standard deviation from a ratio of 1 was calculated from all the cases considered in the simulations. This standard deviation was found to be 0.114, corresponding to 0.47 dB. Since the standard deviation in predicting the SSA performance is less than the standard deviation of repeating the experiments, the simulations predicted the observed performance of the SSA relatively accurately, which is similar to what was found in the beam experiments.

CHAPTER 8

CONCLUSIONS

The work presented here addressed three principle objectives regarding the state-switched absorber used for vibration control: the investigation of the maximum work extraction switching rule, the optimization of the SSA applied the a vibrating continuous system, and the experimental validation of the SSA used to control a vibrating continuous system. The maximum work extraction switching rule, which is designed to maximize the power dissipated by the absorber's damper, does guarantee reduced base motion at the absorber's point of attachment. Also, an optimized state-switched absorber reduces vibrations in continuous systems better than an optimized tuned vibration absorber. This improved performance has been shown through simulations as well as in experiments.

The maximum work extraction switching rule of the state-switching absorber considered by this research is an effective way to control a vibrating system. To reduce vibration in the base to which the SSA is attached, the maximum work extraction switching rule maximizes the power dissipated by the absorber's damper. Since switching has little affect on the power input to the system and all power input to the system must be dissipated by the system's dampers, maximizing the work extracted by the absorber's damper minimizes the base motion. Also, the switching criteria allowing switching to occur only at zero relative displacement of the absorber results in a stable system. The system remains stable because the system energy remains constant across a switch at zero strain. However, switching at the incorrect instant or too slow can lead to

instabilities in the system, as the addition of energy to the system may be necessary to complete the switch.

The state-switched absorber was also optimized to control a vibrating continuous system, specifically a cantilever beam and a clamped plate. The SSA tuning frequencies and location on the beam or plate were optimized using a simulated annealing optimization algorithm and its resulting base system kinetic energy was compared to that of an optimized tuned vibration absorber. The SSA performed as well as, or better, than a classical TVA for the entire range of forcing frequencies of both the beam and the plate systems. At its best, the SSA can reduce the kinetic energy of the beam to which it is attached by 17 dB over that of an optimized TVA. Note, this is a simulation result and the performance of the SSA found by this simulation is highly sensitive to small perturbations in the tuning parameters causing potential difficulties in fabricating an SSA to achieve these large performance gains found by the optimization. The tolerance on frequency performance of the MREs employed to build an SSA is not within the limits implied by these sensitivity results. When the excitation frequencies are near the frequency of the beam's first mode, the optimum attachment point is the free end of the cantilever beam. When the forcing frequencies are near the second mode, the optimum location is near the center of the beam. When optimized for the plate system, the SSA outperforms an optimized TVA by 12.9 dB. The optimal SSA location on a clamped square plate was near the center of the plate for the vast majority of the forcing cases considered. Improved SSA performance is not guaranteed when the optimum tuning frequencies have a large spacing. The best relative performance of the SSA occurred when the optimum tuning frequencies differed by less than a factor of two.

Experiments and simulations were performed to validate the performance of the state-switched absorber used to control vibrating continuous systems, specifically a cantilever beam and a clamped plate. A state-switched absorber was designed using magneto-rheological elastomers (MREs). MREs, which are made from rubber with iron particles suspended throughout, can change stiffness based on the magnetic field applied across them. The SSA built for these experiments had potential for a frequency change of 106%. Both the beam and the plate system were subjected to a two-frequency component excitation. For each forcing case, an experimental direct search of a set of potential tuning frequencies and attachment locations was done to find the best performing SSA as well as the best performing TVA. When applied to a cantilever beam in the experiments, the SSA reduced the beam kinetic energy 2.1 dB versus the beam kinetic energy using a TVA. For the clamped plate experiments, the SSA outperformed the TVA by 2 dB. Simulations of each experimental forcing and tuning case were performed to determine how well the model predicted the experimental results. The error in predicting the observed SSA performance was found to be less then the error in the experiments. Therefore, the numerical simulations predicted results similar to those found in the experiments.

The state-switched absorber has been proven to have improved vibration control performance over classical devices. The zero strain switching criteria used in this work ensures the system will remain stable, while the maximum work extraction switching rule guarantees minimized motion of the body to which it is attached. The SSA has been shown to perform better than a classical TVA at reducing vibrations in both a beam and

plate. These performance gains are observed both through simulations as well as experiments.

REFERENCES

[1] Sun, J. Q., Jolly, M. and Norris, M., "Passive, Adaptive, and Active Tuned Vibration Absorbers-A Survey", *ASME Journal of Vibration and Acoustics*, **Vol. 177**, p. 234-42, 1995.

[2] Den Hartog, J. P., *Mechanical Vibrations*, reprinted by Dover, New York, 1956.

[3] Nashif, A. D., Jones, D. I. G. and Henderson, J. P., *Vibration Damping*, John Wiley & Sons, New York, 1985.

[4] O'Regan, S. D., Burkewitz, B., Fuller, C. R., Lane, S. and Johnson, M., "Payload noise suppression using distributed active vibration absorbers", *SPIE Symposium on Smart Structures and Materials*, San Diego, CA, **Vol. 4698**, p. 150-159, 2002.

[5] Davis, C. L. and Lesieutre, G. A., "Actively tuned solid-state vibration absorber using capacitive shunting of piezoelectric stiffness", *Journal of Sound and Vibration*, **Vol. 232**, p. 601-617, 2000.

[6] Okada, Y. and Okashita, R., "Adaptive control of an active mass damper to reduce structural vibration", *JSME International Journal, Series III*, **Vol. 33**, p. 435-440, 1990.

[7] Yoshida, K., Shimogo, T. and Nishimura, H., "Optimal control of random vibration by use of an active dynamic vibration absorber", *JSME International Journal, Series III*, **Vol. 31**, p. 387-394, 1988.

[8] Dosch, J., Lesiutre, G., Koopmann, G. and Davis, C., "Inertial piezoceramic actuators for smart structures", *SPIE Symposium on Smart Structures and Materials*, **Vol. 2447**, p. 14-25, 1995.

[9] Burdisso, R. A. and Heilmann, J. D., "New dual-reaction mass dynamic vibration absorber actuator for active vibration control", *Journal of Sound and Vibration*, **Vol. 214**, p. 817-831, 1998.

[10] Mizuno, T. and Araki, K., "Active dynamic vibration absorber with automatic frequency-tracking performance", *Transactions of the Japan Society of Mechanical Engineers*, **Vol. 63**, p. 2616-2621, 1997.

[11] Walsh, P. L. and Lamancusa, J. S., "A variable stiffness vibration absorber for minimization of transient vibrations", *Journal of Sound and Vibration*, **Vol. 158**, p. 195-211, 1992.

[12] Lai, J. S. and Wang, K. W., "Parametric control of structural vibration via adaptable stiffness dynamic absorbers", *ASME Journal of Vibration and Acoustics*, **Vol. 118**, p. 41-47, 1996.

[13] Hrovat, D., Baral, P. and Rabins, M., "Semi-active versus passive or active tuned mass dampers for structural control", *ASCE Journal of Engineering Mechanics*, **Vol. 109**, p. 691-705, 1983.

[14] Abe, M. and Igusa, T., "Semi-active dynamic vibration absorbers for controlling transient response", *Journal of Sound and Vibration*, **Vol. 198**, p. 547-569, 1996.

[15] Nguyen, P. H., *An exploration of parametric excitation as a tool for vibration control*, Ph. D. Dissertation, Georgia Institute of Technology, Atlanta, 2000.

[16] Bender, E. K., "Optimum linear preview control with application to vehicle suspension", *ASME Journal of Basic Engineering*, **Vol. 90**, p. 213-221, 1968.

[17] Krasnicki, E. J., "Comparison of analytical and experimental results for a semi-active vibration isolator", *The Shock and Vibration Bulletin*, **Vol. 50**, p. 69-76, 1980.

[18] Karnopp, D., "Design principles for vibration control systems using semi-active dampers", *ASME Journal of Dynamic Systems, Measurement and Control*, **Vol. 112**, p. 448-455, 1990.

[19] Simon, D. E. and Ahmadian, M. E. V. T., "An alternative semiactive control method for sport utility vehicles", *Proceedings of the Institution of Mechanical Engineers, Part D: Journal of Automobile Engineering*, **Vol. 216**, p. 125-139, 2002.

[20] Rajamani, R. and Hedrick, J. K., "Performance of active automotive suspensions with hydraulic actuators: theory and experiment", *Proceedings of the 1994 American Control Conference*, Baltimore, MD, **Vol. 2**, p. 1214-1218, 1994.

[21] Lee, H.-S. and Choi, S.-B., "Control and response characteristics of a magneto-rheological fluid damper for passenger vehicles", *Journal of Intelligent Material Systems and Structures*, **Vol. 11**, p. 80-87, 2000.

[22] Bakhtiari-Nejad, F. and Karami-Mohammadi, A., "Active vibration control of vehicles with elastic body, using model reference adaptive control", *Journal of Vibration and Control*, **Vol. 4**, p. 463-479, 1998.

[23] Hrovat, D. and Hubbard, M., "Optimum Vehicle Suspensions Minimizing Rms Rattlespace, Sprung-Mass Acceleration and Jerk", *Journal of Dynamic Systems, Measurement and Control*, **Vol. 103**, p. 228-236, 1981.

[24] Gavin, H. P. D., Nitin S., "Resonance suppression through variable stiffness and damping mechanisms", *SPIE Conference on Smart Systems for Bridges, Structures, and Highways*, Newport Beach, CA, **Vol. 3671**, p. 43-53, 1999.

[25] Jacquot, R. G., "Optimal dynamic vibration absorbers for general beam systems", *Journal of Sound and Vibration*, **Vol. 60**, p. 535-42, 1978.

[26] Kitis, L., Wang, B. P. and Pilkey, W. D., "Vibration reduction over a frequency range", *Journal of Sound and Vibration*, **Vol. 89**, p. 559-569, 1983.

[27] Rice, H. J., "Design of multiple vibration absorber systems using modal data", *Journal of Sound and Vibration*, **Vol. 160**, p. 378-385, 1993.

[28] Esmailzadeh, E. and Jalili, N., "Optimum Design of Vibration Absorbers for Structurally Damped Timoshenko Beams", *Journal of Vibration and Acoustics*, **Vol. 120**, p. 833-841, 1998.

[29] Hadi, M. N. S. and Arfiadi, Y., "Optimum design of absorber for MDOF structures", *Journal of Structural Engineering*, **Vol. 124**, p. 1272-1279, 1998.

[30] Davis, C. L., Lesieutre, G. A. and Dosch, J., "A tunable electrically shunted piezoceramic vibration absorber", *SPIE Symposium on Smart Structures and Materials*, San Diego, CA, **Vol. 3045**, p. 51-59, 1997.

[31] Clark, W. W., "Semi-active vibration control with piezoelectric materials as variable stiffness actuators", *SPIE Symposium on Smart Structures and Materials*, Newport Beach, CA, **Vol. 3672**, p. 123-130, 1999.

[32] Richard, C., Guyomar, D., Audigier, D. and Ching, G., "Semi-passive damping using continuous switching of piezoelectric devices", *SPIE Symposium on Smart Structures and Materials*, Newport Beach, CA, **Vol. 3672**, p. 104-111, 1999.

[33] Larson, G. D. and Rogers, P. H., "State switched acoustic source", *Journal of the Acoustical Society of America*, **Vol. 96**, p. 3317(A), 1994.

[34] Larson, G. D., *The analysis and realization of a state switched acoustic transducer*, Ph.D. Dissertation, The Georgia Institute of Technology, Atlanta, GA, 1996.

[35] Larson, G. D., Rogers, P. H. and Munk, W., "State switched transducers: A new approach to high-power, low-frequency, underwater projectors", *Journal of the Acoustical Society of America*, **Vol. 103**, p. 1428-1441, 1998.

[36] Larson, G. D. and Cunefare, K. A., "Experimental investigation of control logic for State-switched dampers", *18th Biennial Conference on Mechanical Vibration and Noise*, Pittsburgh, PA, **Vol. 6 B**, p. 1353-1358, 2001.

[37] Kurdila, A. J., Clark, W. W., Wang, W. and McDaniel, D. E., "Stability of a Class of Real-Time Switched Piezoelectric Shunts", *Journal of Intelligent Materials Systems and Structures*, **Vol. 13**, p. 107-116(10), 2002.

[38] Davis, C. L. and Lesieutre, G. A., "A modal strain energy approach to the prediction of resistively shunted piezoceramic damping", *Journal of Sound and Vibration*, **Vol. 184**, p. 129-139, 1995.

[39] Ginder, J. M. N., M.E.; Elie, L.D.; Clark, S.M, "Controllable-stiffness components based on magnetorheological elastomers", *SPIE Symposium on Smart Structures and Materials*, Newport Beach, CA, **Vol.** p. 418-425, 2000.

[40] Cunefare, K. A., De Rosa, S., Sadegh, N. and Larson, G., "State-switched absorber for semi-active structural control", *Journal of Intelligent Material Systems and Structures*, **Vol. 11**, p. 300-310, 2000.

[41] Holdhusen, M., *Experimental Validation and the Effect of Damping on the State-Switched Absorber Used for Vibration Control*, MS Thesis, Georgia Institute of Technology, Atlanta, GA, 2002.

[42] Meirovitch, L., *Elements of vibration analysis*, McGraw-Hill, New York, 1986.

[43] Young, D., "Vibration of Rectangular Plates by the Ritz Method", *Journal of Applied Mechanics*, **Vol. 17**, p. 448-53, 1950.

[44] Metropolis, N., Rosenbluth, A., Rosenbluth, M., Teller, A. and Teller, E., "Equation of State Calculations by Fast Computing Machines", *Journal of Chemical Physics*, **Vol. 21**, p. 1087-92, 1953.

[45] Kirkpatrick, S., Gelatt, C. D. and Vecchi, M. P., "Optimization by Simulated Annealing", *Science*, **Vol. 220**, p. 671-80, 1983.

[46] Albanese, A. M. and Cunefare, K. A., "Properties of a magnetorheological semiactive vibration absorber", *SPIE Symposium on Smart Structures and Materials*, San Diego, CA, **Vol. 5052**, p. 36-43, 2003.